STAINLESS STEEL MEMBRANE CHARACTERIZATION AND AQUEOUS TRANSPORT STUDIES

By
Richard L. Ames

A thesis submitted to the Faculty and Board of Trustees of the Colorado School of Mines in partial fulfillment of the requirement for the degree of Masters of Science (Chemical Engineering and Petroleum Refining).

Golden, Colorado

Date 10-23-01

Signed: Richard L. Ames

Richard L. Ames

Approved: J. Douglas Way

Dr. J. Douglas Way
Thesis Advisor

Golden, Colorado

Date 10-23-01

James F. Ely

Dr. James F. Ely
Professor and Head
Department of Chemical Engineering
And Petroleum Refining

ABSTRACT

The purpose of this study was to initiate investigations into the feasibility of using porous stainless steel membranes to selectively remove actinide and non-actinide cation constituents from waste solutions. The membrane material used for initial testing, purchased from Mott® Metal Corporation, was a sintered 316L stainless steel membrane having a nominal filtration rating of 0.5 μm the and thickness of approximately 0.123 cm. Experimentation was conducted in two phases beginning with physical characterization of the membrane material and then measurement of transport through the membrane material with non-atinide (Cs^{+}, Ca^{2+} and Eu^{3+}) and actinide (Am^{3+}, and Pu^{4+}) cations under dilute conditions. Tests confirmed that diffusion was the rate controlling mechanism for transport through the membrane. Characterization experimentation was conducted at the Colorado School of Mines in the Chemical Engineering Department (CEPR) whereas, radiotracer transport experimentation was conducted at Technical Area 48, Los Alamos National Laboratory.

Characterization tests were conducted to determined the pore size distribution, porosity, and toruosity of the stainless steel membrane material. The average pore size was approximately 2.2 μm and the average the porosity was 24.9 %. The tortuosity, determined by conducting transport studies of ^{14}C-labeled sucrose through the stainless steel membrane, was estimated to be 1.30.

Results from transport experimentation confirmed diffusion as the rate controlling mechanism for the transport of cation solutes through the stainless steel membrane as experimentally determined infinite-dilution diffusion coefficients (D_0) compare well with those found in referenced literature. For monovalent cesium (Cs^+), the D_0 found in literature was determined to be 10.0×10^{-6} cm^2/s compared to an experimentally determined value of $7.0\times10^{-6} \pm 2.6\times10^{-6}$ cm^2/s. For divalent calcium (Ca^{2+}), the referenced D_0 value of 7.9×10^{-6} cm^2/s is slightly higher than the experimentally determined value of $4.5\times10^{-6} \pm 2.0\times10^{-6}$ cm^2/s. Finally, for trivalent ions europium (Eu^{3+}) and americium (Am^{3+}), the coefficients (D_0) found in literature are 5.18×10^{-6} cm^2/s and 6.25×10^{-6} cm^2/s, respectively, which compare well with the coefficients determined experimentally ($3.7\times10^{-6} \pm 2.9\times10^{-6}$ cm^2/s and $4.5\times10^{-6} \pm 1.8\times10^{-6}$ cm^2/s for Eu and Am, respectively).

In addition, the infinite-dilution diffusion coefficient for plutonium as $Pu(OH)^{3+}$ (which was not available in reference literature) was determined to be $3.3x10^{-6} \pm 1.3x10^{-6}$ cm^2/s.

TABLE OF CONTENTS

LIST OF FIGURES

LIST OF TABLES

ACKNOWLEDGEMENTS

I would like to express appreciation to the personnel of the Department of Energy and the Los Alamos National Laboratory for sponsorship without which this project would not have been possible. In particular, a great deal of thanks to Steve Schreiber and Steve Yarbro for their encouragement and support, not only technically and financially, but emotionally. Special thanks to my mentors Liz Bluhm and Kent Abney for their support and flawless guidance, providing laboratory and office space, taking samples, and so much more (including your friendship). I would also like to give special thanks to Dr. Doug Way for his patience, encouragement, ideas, time and wholehearted interest in this work (even though it was aqueous), as you made the journey enjoyable.

Finally, I would like to express my most heartfelt appreciation to my family Scott, Joan, Al, Jeff, Laura, Donna and Dan for your enduring endorsement. Your confidence in me was truly invaluable.

Chapter 1 INTRODUCTION

Los Alamos National Laboratory aqueous processing facilities use a number of unit operations to separate actinide contaminants from waste solutions. The objective of this study was to begin preliminary investigations into the feasibility of using porous stainless steel membranes to selectively remove actinide and non-actinide cation constituents from waste solutions so that the waste can be discarded to the liquid waste treatment facility. The general experimental plan followed was to initially determine the physical characteristics of the membrane material and then to examine the transport properties of the membrane material with actinide (Am^{3+}, and Pu^{4+}) and non-actinide cations (Cs^{+}, Ca^{2+} and Eu^{3+}) under dilute conditions. The purpose of characterization studies was to enable researchers to predict transport behavior and explain diffusion anomalies following transport experimentation, whereas transport studies were conducted to determine if the membrane hindered or influenced the diffusion of a solute. The hypothesis was that diffusion as the rate controlling mechanism. The investigations were conducted at the Colorado School of Mines in Golden, Colorado, and at Los Alamos National Laboratory in Los Alamos, New Mexico.

1.1 Background

Aqueous processing is conducted at the Los Alamos National Laboratory for the purpose of removing actinide and non-actinide constituents from solid and liquid waste streams. Nitric acid and hydrochloric acid based unit operations, such as dissolution, ion exchange, precipitation, solvent extraction and calcination, are used to remove various constituents. Although the hydrochloric acid based system is very efficient for materials that are difficult to process, equipment materials of construction tend to be expensive and difficult to manufacture and repair. However, material compatibility issues are not prevalent with the nitric acid system and a large portion of the system components can be constructed from glass or stainless steel. As a result, the majority of the actinide separation processing is conducted in the nitric acid system.

Los Alamos personnel are continuously searching for unit operation improvements or new process ideas for the nitric acid system and one field of interest has long been membrane technology. Recent investigations have centered around the generation of facilitated transport membranes constructed on an alumina membrane support (Bluhm 1999; Bluhm 2000). Investigations have been completed with an unmodified alumina membrane material (0.02 and 0.1 μm nominal pore diameter) resulting in basic membrane physical characterization and cation transport data in preparation for chemical modification of the membrane. Now that this research has been concluded, work is underway to chemically modify the membrane and initiate transport experimentation. Unfortunately, the alumina membrane support has limitations in even the nitric acid system as the material will not survive in an acidic environment. Because of the limitations of the alumina membrane, a search was initiated for a robust membrane material that could be modified for facilitated transport in an acidic environment. The material chosen for this work was a stainless steel membrane support material manufactured by Mott® Corporation, (Farmington, Connecticut). The material is acid resistant and can be described as a sintered 316L stainless steel membrane having a nominal filtration rating of 0.5 μm (generally defined as 90 % of particulate material of this diameter or larger is removed in an aqueous environment). Additional specifications for the Mott® 316 stainless steel material are listed in Table 1.1.

Table 1.1 - Mott® Stainless Steel Membrane Spcifications*

Material of Construction	316L Stainless Steel
Nominal Filtration Rating (90%)	0.5 μm
Filter Classification	Microfilter (pore diameter > 0.1 μm)
Pore Size Distribution	2 to 3 μm
Membrane Thickness	0.123 cm

* Mott® Metal Corporation

The stainless steel membrane sheet material was manufactured by a process which begins with sieved metal powder that is compressed into the desired shape, then sintered at approximately 1200°C in a positive-pressure hydrogen furnace. The hydrogen atmosphere minimizes the surface oxide film that is formed during the sintering process. Particle sieving and control of the manufacturing process results in the ability to control the density and pore size of the membrane material. The stainless steel material was purchased from the manufacturer in sheets and machined into 2.5 cm diameter disks at the Los Alamos National Laboratory.

1.2 Characterization of the Mott® Stainless Steel Membrane

Membrane characterization tests were conducted to determined the pore size (diameter) distribution or mean pore size, the porosity (void volume), and toruosity (actual diffusion path length through the membrane compared to the membrane thickness) of the stainless steel membrane material. These characteristics were used to predict transport behavior and explain diffusion anomalies observed during transport experimentation. In general, the molecular diffusion rate of a given solute through the membrane approaches the bulk diffusivity as the pore size and the porosity increase, and the transport rate increases as the tortuosity decreases. Membrane characterization experimentation was conducted at the Colorado School of Mines in the Chemical Engineering and Petroleum Refining Department (CEPR) facilities.

Optical microscopic (microscopic photography) digital gray scale analysis was conducted with cross-sectioned stainless steel membrane material as a method of estimating characteristics and confirming results of the more precise characterization analyses. Cross-section preparation and optical microscopy photography was conducted by personnel in the Material Science Technology Division at the Los Alamos National Laboratory.

All characterization experiments were conducted with unmodified (bare) stainless steel membrane material that was subject to a pre-characterization cleaning process. The material was cleaned using a three step process (detailed in Appendix I.1) which consisted of solvent/oil removal by cleansing in an ozone cleaner, etching the surface with 25% HCl, and an ultrasonic water wash. The cleaning process was developed by Los Alamos National Laboratory experts and was to be used in preparation of the membrane for all characterization and transport experimentation and is planned to be used prior to any membrane surface modification for future transport studies.

1.2.1 Pore Size Distribution

The pore size and pore size distribution was determined by conducting experimentation based on the Young-La Place bubble point equation. The experiment measures the differential gas flow through a liquid saturated membrane and the gas flow through the same dry membrane. The final results of this analysis are the relative percentages of pore diameters from which both the mean pore size and the distribution can be estimated (ASTM E1294-89 (1999) 1999).

1.2.2 Porosity

The porosity is defined as the percentage void volume of a material. The concept of measuring the porosity is simple in that a dry membrane is submerged in a liquid essentially displacing any gas present in the void volume. The porosity is calculated based on the change in mass and the densities of the membrane and liquid. An important factor in determining an accurate porosity is that a liquid with a low surface tension be used so that a high percentage of void volume gas will be displaced. Ideally, the wetting of the membrane material should be conducted in a chamber under moderate vacuum in order to maximize gas remove from membrane pores.

1.2.3 Tortuosity

The membrane tortuosity (τ) is defined as the ratio of the actual diffusion path length across the membrane divided by the thickness of the membrane (Mulder 1998). Figure 1.1 illustrates the tortuosity for three pores of different length through a membrane of thickness t. The tortuosities determined for the stainless steel membrane are based on an average of all path lengths.

Figure 1.1 – Membrane Tortuosity

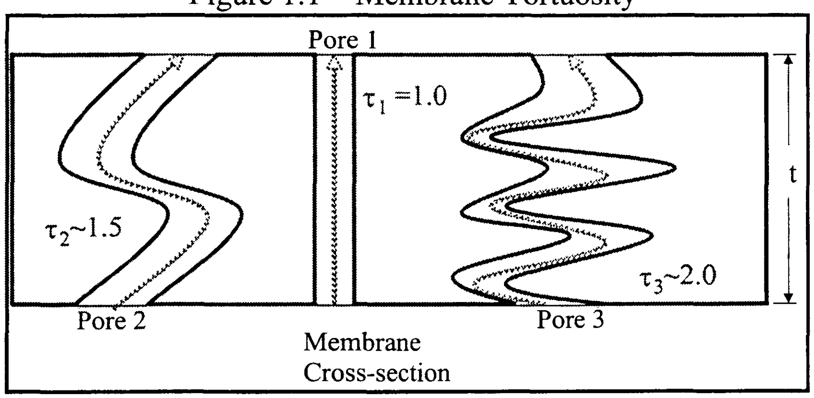

The tortuosity was determined by comparing the published infinite-dilution diffusion coefficient data for sucrose to the effective diffusion coefficient for sucrose through the membrane. The effective diffusion coefficient for sucrose was determined experimentally by conducting radiotracer transport studies with ^{14}C-labeled sucrose through the stainless steel membrane.

1.2.4 Summary of Characterization Results

Chapter 2, Stainless Steel Membrane Characterization, provides details of the experimental procedures, results, and provides a discussion and conclusions for the characterization of the Mott® 316 stainless steel membrane material. In summary, experimental results indicated that the average pore size was approximately 2.2 ± 0.5 μm, and the average the porosity of the membranes tested was estimated to be 24.9 ± 5.2 %. Tortuosity experimental data resulted in an estimated tortuosity 1.30 ± 0.07 (unitless) for the membrane material. All variability (±) reported are calculated as the 95% confidence interval.

1.3 Transport Characterization

The objective of cation diffusion transport studies was to determine if the stainless steel membrane material influenced diffusion of given solutes through solution. Prior to initiating laboratory research, the hypothesis was made that diffusion was the controlling mechanism of transport through the membrane due to of the large size of the material pores. In other words, solute diffusion would not be influenced by the membrane surface (other than the effect of increased diffusional path length).

Of primary concern was the possibility of electrochemical wall effects influencing the cation diffusion rate. Experiments were designed to determine if the cation effective diffusion coefficient could be a function of the electrostatic charge of the membrane surface by examining cation solutes of varying charge, and by varying the initial pH of transport experiments for a given cation solute. The diffusive flux of cationic solutes through the sintered stainless steel membranes were determined and compared. Analytical equations for the transport system were developed for the purpose of determining experimental effective diffusion coefficients for the cation solutes. These mathematical relationships were developed from fundamental transport phenomena relationships such as Fick's Law of flux, the system mass balances and the concentration driving force for a mass transport system assuming dilute solutes.

1.3.1 Experimental Effective Diffusion Coefficients

Standardized procedures were developed (Appendix I.2) and used to conduct radiotracer cation (and for ^{14}C-labeled sucrose) transport experimentation in a batch transport apparatus constructed with feed and permeate cells separated by a stainless steel membrane disk. Cations chosen for testing, Cs^{+}, Ca^{2+}, Eu^{3+}, Am^{3+}, and Pu^{4+}, were selected based on cation charge, based on those cations expected under actual process conditions, and on cations chosen for similar experimentation (Bluhm 1999; Bluhm 2000). The initial total ionic concentrations varied between experiments depending on the cation, initial experimental pH, and amount of pH adjustment required (resulting from the addition of NaOH or HNO_3). Initial transport apparatus liquid volumes were uniform between tests. Finally, initial feed cell concentrations of the tracer cation ranged between approximately 10^{-7} and 10^{-12} M.

Experimental data were used to determine the effective diffusion coefficient as briefly explained above. Included in Chapter 3, Stainless Steel Membrane Transport

Studies, is a summary of the cation effective diffusion coefficients, a detailed discussion of results, a summary of results, and conclusions.

1.3.2 Analysis of Results

A comprehensive discussion of the results of all transport experimentation is also included in Chapter 3. Experimentally determined (infinite-dilution) effective diffusion coefficients are compared to those found in literature with a favorable outcome. Also discussed is the relationship between the electrostatic surface charge of the ionic membrane material and it's effect (or lack of effect) on cation effective diffusion coefficients through the material. Also detailed is an analysis of the possible diffusional resistance caused by the configuration of the transport apparatus, as well as a summary of observed drift in the initial pH of the transport systems for those systems at near-neutral conditions.

1.3.3 Summary of Transport Experimental Results

The primary observation from experimental transport experimentation is that the infinite-dilution diffusion coefficients determined from transport experimentation compare favorably to infinite-dilution diffusion coefficients from referenced literature for Eu^{3+}, Am^{3+}, Cs^{+}, and Ca^{2+}. In addition, no significant variance was observed in the experimentally determined effective diffusion coefficient for any of the given cations over the range of pH investigated. These results support the hypothesis that diffusion is the rate controlling mechanism, or that the bare membrane material does not influence the diffusion of the cation examined.

1.4 Final Conclusions and Recommendations

A summary of all experimentation, conclusions and recommendations is included in Chapter 4, Summary. This chapter attempts to bring together the information gathered during all three phases of the task completed which include stainless steel membrane characterization, development of transport characteristics, and data analysis. Recommendations are based on lessons learned from the research and range from alternate methods of data analysis to those derived from experimental difficulties.

Chapter 2 STAINLESS STEEL MEMBRANE CHARACTERIZATION

2.1 Introduction

This chapter provides detailed information on the characterization of Mott® stainless steel membrane material to be used in cation transport studies at Technical Area 48, Los Alamos National Laboratory. The 316 stainless steel membrane material used for testing was purchased from Mott Metal Corporation®. The nominal filtration rating was specified by the manufacturer as less than 0.5 μm, with an estimated pore size distribution from 2 to 3 μm and membrane thickness measured to be between 0.123-0.124 cm (using a calibrated hand-caliper) for the actual material used during experimentation (Mott® Metal Corporation).

Membrane characterization tests were conducted to determine the pore size distribution, the porosity (void volume), and toruosity of the stainless steel membrane material. Results indicate that the average pore size was approximately 2.2 ± 0.5 μm, and the average porosity of the 36 membranes tested was 24.9 ± 5.2 %. The tortuosity, determined by conducting radiotracer transport studies of for ^{14}C-labeled sucrose through the stainless steel membrane, was estimated at 2.1 ± 0.5 (unitless).

2.2 Experimental

Membrane disks (25 mm diameter) used during experimentation were cut from sheet material by Los Alamos personnel. The material was cleaned using a three step process (detailed in Appendix I.1) which consisted of solvent/oil removal by cleansing in an ozone cleaner for 20 minutes, etching the surface with 25% HCl for 5 minutes, and a water (DI) wash in an ultrasonic cleanser for 24 hours. Membrane characterization experimentation was conducted at the Colorado School of Mines in the Chemical Engineering and Petroleum Refining Department (CEPR) research facilities. All characterization experiments were conducted with unmodified (bare) stainless steel membranes. Optical microscopy photography and membrane cross-section preparation were conducted by personnel in the Material Science Technology Division at the Los Alamos National Laboratory.

2.2.1 Pore Size Distribution

Membrane pore size distribution can be estimated using the simple gas flow (or flow porometer) apparatus illustrated in Figure 2.1. The basic test procedure used requires monitoring the nitrogen outlet flow rate from the 25 mm Millipore® membrane cell apparatus (containing the stainless steel membrane) as a function of the feed gas pressure. A detailed description of the pore size distribution mean pore diameter experimental procedure is located in Appendix I.3 (ASTM E1294-89(1999) 1999). The Young-Laplace bubble point equation (Equation 2.1) was used to calculate the pore size from the pressure difference data (Burggraaf 1996).

$$D_{P_i} = \frac{4\gamma}{\Delta P_i} \qquad \text{Equation 2.1}$$

Where D_{pi} = Diameter of membrane pore (μm).
γ = Surface tension of solvent (dyne/cm).
ΔP_i = Pressure differential (psig).

Prior to experimentation, the membrane to be characterized is saturated with a given solvent (2-isopropanol). First, the porometer gas flow experiment was conducted with the "wet," or solvent saturated membrane, measuring the gas flow rate as a function of feed pressure (ΔP_i). Nitrogen exit flow data was again gathered after the membrane had been dried for 1 hour by flowing nitrogen through the membrane at the rate of approximately 15 L/minute.

Figure 2.1 – Membrane Porometer

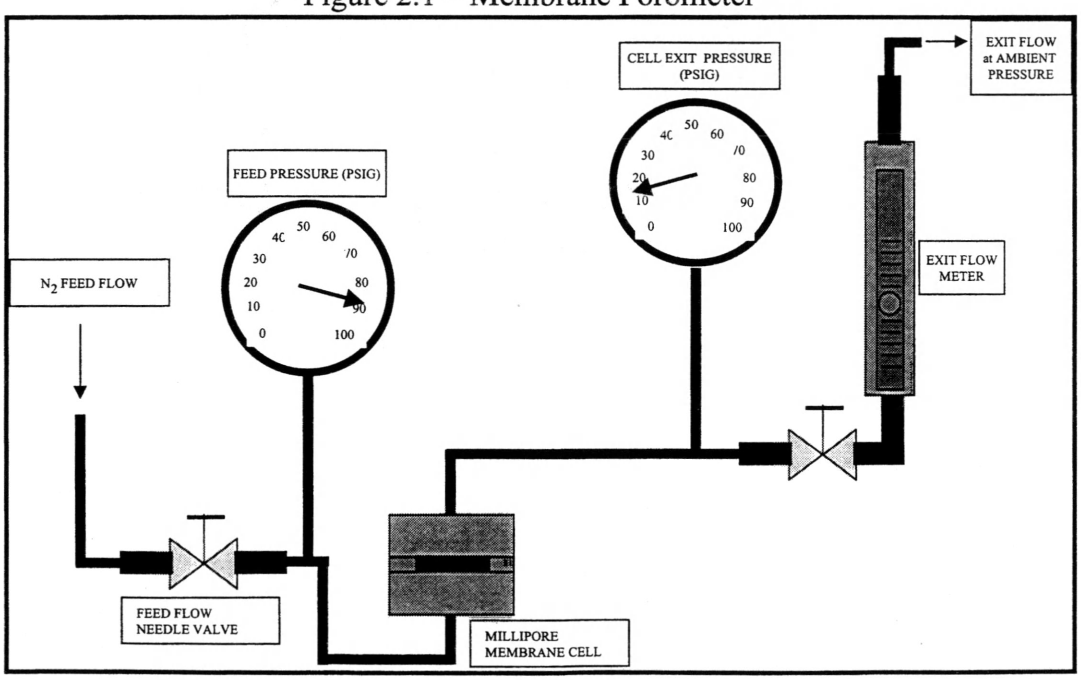

The percentage of differential flow through the membrane was then estimated from the differential flow using Equation 2.2. The flow through the flow meter was calculated from the calibration data generated by the meter manufacturer.

$$\%\ \text{Differential Flow}_i = 50[(\frac{F_w}{F_d})_{i+1} - (\frac{F_w}{F_d})_{i-1}] \qquad \text{Equation 2.2}$$

Where % Diff. Flow = % of total flow through the membrane ΔP_i.
(estimate of % of a given pore size in a membrane).
F_w = Flow through wet membrane.
F_d = Flow through dry membrane.
i-1 = Flow data at previous feed pressure.
i+1 = Flow data at next feed pressure.

By plotting the percentage differential flow through a membrane against the pore diameter, an illustration of the relative pore diameter can be generated. In addition, the mean pore diameter can be estimated as the pore diameter at the peak of the percentage differential flow value on the figure (Mietton-Peuchot 1997; Jena 1999; ASTM E1294-89(1999), 1999). However, for purposes of our experimentation, the mean pore diameter was calculated using an area-average graphical analysis method.

2.2.2 Porosity

A number of Mott® stainless steel membranes were cleaned using the procedure (ozone, HCl, followed by sonic cleaning) as outlined in Appendix I.1. The membranes were dried, for no less than 1 hour by flowing nitrogen through the membrane at a rate of approximately 15 L/minute, and then weighed. Each membrane was then soaked in 2-isopropanol for 3 days and again weighed. The mass difference was then calculated and the porosity calculated based on the fluid density. A detailed description of this procedure is located in Appendix I.4.

2.2.3 Tortuosity

Tortuosity (τ) is defined as the diffusional path length through a pore divided by the thickness of the membrane. Figure 1.1 (Chapter 1, Introduction) illustrates the definition of tortuosity by showing three pores with varying lengths. Stated differently, the tortuosity accounts for the actual distance that the solute must travel in the pores of the membrane. Values of tortuosity for a porous membrane with periodically spaced, irregular shaped, impermeable particles, range from 3 to 6 but have been observed as high as 10 (Cussler 1997).

One method of determining the tortuosity involves using the measured, or effective, diffusion coefficient, the porosity and a known diffusion coefficient in dilute solution with no membrane. Equation 2.3 shows the relationship used to calculate the tortuosity.

$$\tau = \frac{\varepsilon D_o}{D_{eff}} \qquad \text{Equation 2.3}$$

Where τ = Tortuosity (unitless).
D_o = Diffusion coefficient with no membrane (cm^2/s).
D_{eff} = Measured diffusion coefficient with membrane (cm^2/s).
ε = Porosity (unitless).

Diffusion coefficients were measured for ^{14}C-labeled sucrose under dilute aqueous conditions (2×10^{-8} M). Each transport test designed to determine the measured effective diffusion coefficient (D_{eff}) was conducted in the transport apparatus illustrated in Figure 2.2. The transport cell consisted of a feed cell joined to a permeate cell (each cell being approximately 250 mL in volume filled with 100 mL of solution) by a bridge containing the stainless steel membrane disk. Both feed and permeate cells of the apparatus were mixed with a magnetic stirrer at a rate of 300 rpm. Individual experimental testing periods ranged from 10 days to 2 weeks.

Preliminary transport characteristic comparisons were conducted by measuring the change of the sucrose concentration in both the permeate and feed cells as a function of time (Cussler 1997). Radiotracer sample activities (concentrations) were determined by β-emission counting using a Wallac Liquid Scintillation Counter, model 1414, for ^{14}C-labeled sucrose. Using Fick's Law, system mass balances and the driving force, a relationship was developed between the concentration and the diffusion coefficient (D_{eff}) as shown in Equation 2.4. The detailed development of this equation can be found in Section 3.2.4.

Figure 2.2 – Transport Experimental Test Apparatus

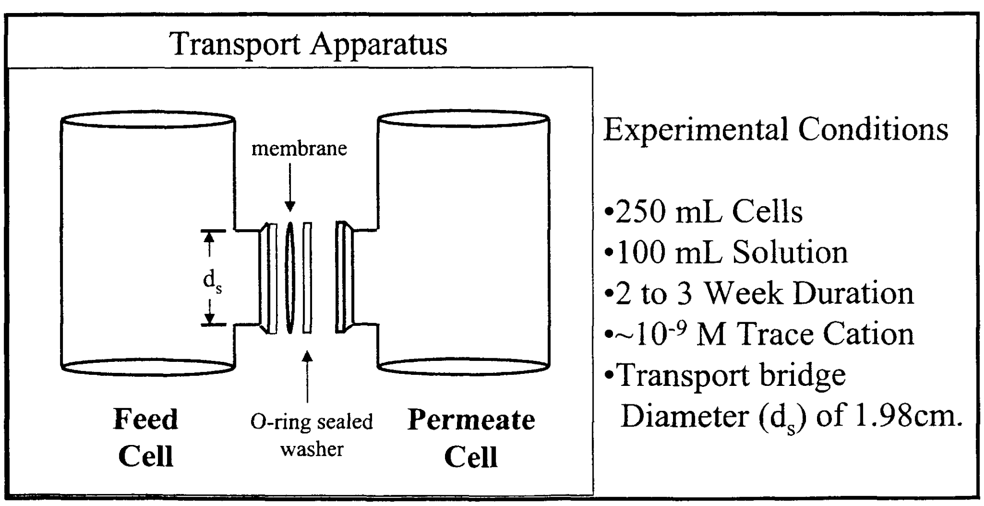

$$\frac{V_f l}{2S} ln(\frac{A_{fo}}{A_f - A_r}) = D_{eff} t$$ Equation 2.4

Where V_f = Volume of the feed side cell (cm^3).
S = Membrane surface area in contact with fluid (cm^2).
A_r = Activity (cpm) of the retentate at time t (s).
A_f = Activity (cpm) of the feed at time t (s).
A_{fo} = Activity (cpm) of the feed at t=0.
D_{eff} = Cation diffusion coefficient (cm^2/s).
l = Membrane thickness (cm).

The diffusion coefficients were calculated from the slope of the least squares regression analysis of the left hand side of Equation 2.4 with time, allowing for a non-zero time intercept and allowing for the contribution of bulk flow in the first few hours of the experiment. For the same reason, data from the first 48 hours were not included with the regression analysis.

For the purpose of determining if experimental values were reasonable, an estimate of the tortuosity of the stainless steel membrane material was calculated prior to experimentation from a model which assumed that the stainless steel is composed of impenetrable spheres using Equation 2.5 (Cussler 1997). Assuming the stainless steel membrane porosity to be 25% (sphere volume fraction is 0.75), we estimate the tortuosity of this material to be approximately 1.4.

$$\tau = \frac{(3-\varepsilon)}{2}$$ Equation 2.5

Where τ = Tortuosity (unitless).
ε = Porosity (unitless).

2.3 Results and Discussion

Results from information gathered during the pore size distribution, porosity, and tortuosity characterization experiments are detailed below. Statistical error is reported for a 95 % confidence interval unless noted otherwise (Moore 1989; Gorden 1972).

2.3.1 Pore Size Distribution

Figure 2.3 illustrates the pore size distribution as a function of the percentage of the given pore size (percent differential gas flow) for stainless steel membrane number N19. From Figure 2.3 the mean pore diameter can be estimated as the peak percentage (%) differential flow value. Here the mean pore diameter is estimated to be 2.1 μm with the pore size ranging from 1.3 μm to 4.2 μm (ASTM E1294-89 (1999) 1999). The mean pore diameter can also be estimated more accurately using a method from the differential flow plot which calculates an area average. Using this method, the results for membrane N19 was determined to be 2.2 μm.

Twenty (20) stainless steel membranes were characterized using the flow porometer (using 2-isopropanol as the test solvent) with consistent pore distribution and mean pore diameter results. On average for the experiments using 2-isopropanol (IP) as the test solvent, the mean pore diameter for these membranes was determined to be 2.2 ± 0.5 μm. This result is consistent with the manufacturer specification that the pore diameter is between 2 and 3 μm.

Figure 2.3 - Pore Size Distribution Results Using 2-isopropanol (Membrane N19)

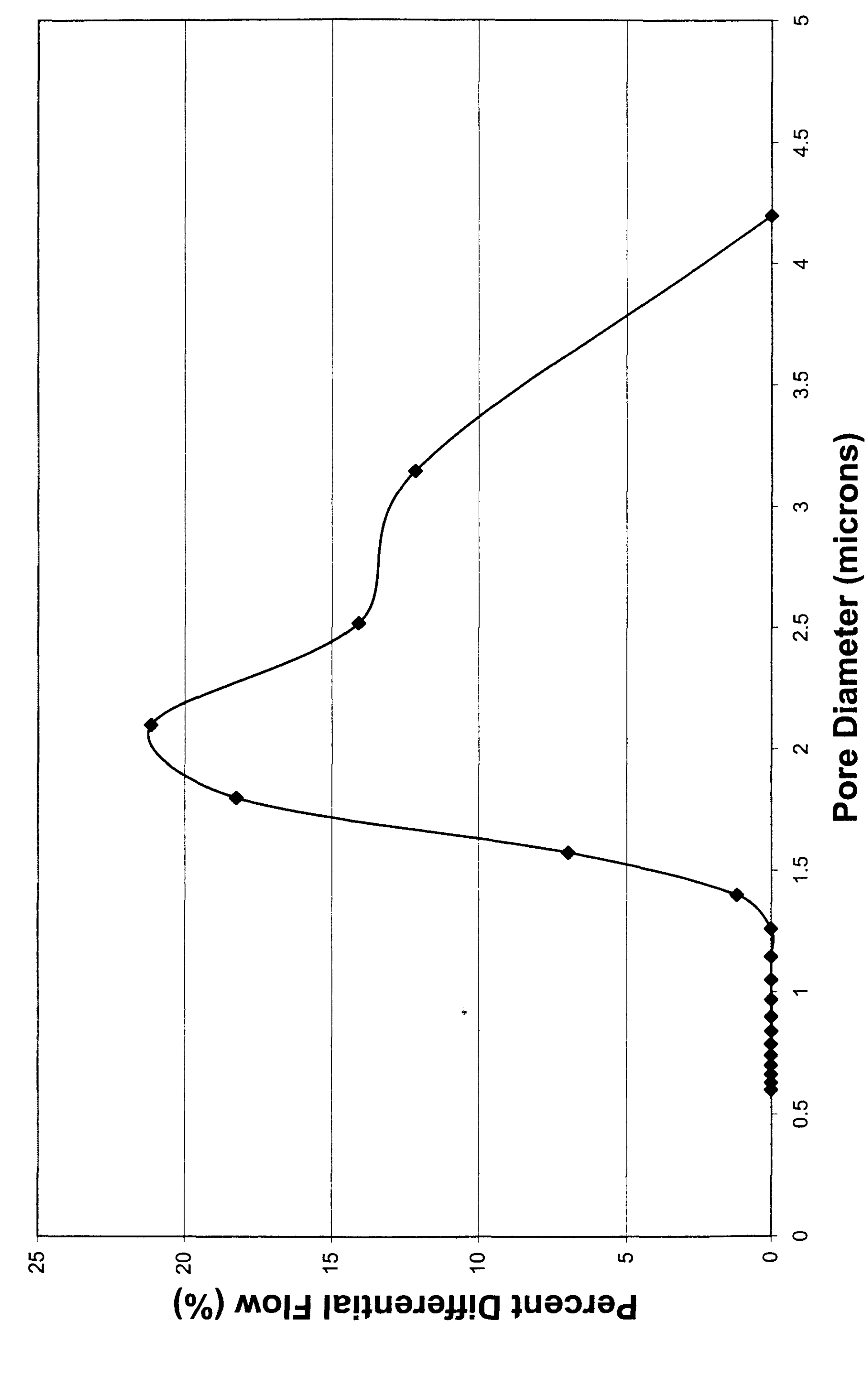

The experimentally determined pore size distribution for the membranes was determined to be between 0.7 μm to 6.3 μm with the average range being between 1.2 μm to 3.6 μm. This large pore size distribution is not consistent with the manufacturer specifications in that the range is significantly larger than that indicated by the Mott® Metal Corporation. Table 2.1 summarizes the results of the pore size distribution experiments, whereas, detailed pore size distribution data is located in Appendix II for all membranes tested. The median pore diameter (the mean pore diameter that occurs most often) is estimated to be 1.3 μm for this population of Mott® stainless steel membranes.

In comparison, experimentally determined average pore diameter and pore size distribution determined during this study using porometry compare well with results from similar studies. Using a static bubble point method, Ma and Mardilovich reported the Mott® 0.5 μm stainless steel membranes characteristic pore size distribution as between 1.4 and 8 μm, and the average pore diameter of approximately 2.5 μm (Mardilovich 1998, Ma 2001).

Table 2.1 – Pore Size Distribution Data

Membrane Solvent	Mean Pore Diameter - D_D (μm)	Average Distribution (μm)
2-Isopropanol	2.2 ± 0.5	1.2-3.6

2.3.2 Porosity

Thirty six (36) Mott® stainless steel membranes were cleaned and porosity measurements were conducted using the procedure detailed in Appendix I.4. Results indicated that, on average for experiments using 2-isopropanol as the test solvent, the porosity of these membranes was approximately 24.9 ± 5.2%. Original estimates were that the porosity would be as high as 40%. Table 2.2 summarizes the porosity data that were obtained, and detailed porosity data is listed in Appendix III (Table A-2, Porosity Data).

Table 2.2 – Porosity Data

Porosity Experiment Solvent	Void (%)
Average De-ionized Water (DI)	17.1± 4.8
Average 2-Isopropanol (IP)	24.9 ± 5.2

Note: Solvent soak time predominantly 3 days.

Results using 2-isopropanol as the test solution indicate that the porosity is approximately 28% higher than results using DI water. This difference is probably the result of the fact that 2-isopropanol has a lower surface tension than DI water (i.e. more solution will penetrate the membrane pores at a lower pressure with a solution that is a lower surface tension) as shown by Equation 2.1. It was for this reason that experimental data gathered using water were not used when determining final statistical mean porosity.

Porosity experiments were repeated on 10 stainless steel membranes for the purpose of determining the error involved with the experimental procedure as compared to the porosity variability between membranes. Each of the ten membranes were nitrogen dried for 1 hour, weighed, soaked in 2-isopropanol for 5 days, and again weighed. The membranes were then placed back in the solvent and again weighed at 7 and 10 days (membranes were not dried after 5 and 7 day weighing). For the 10 membranes examined, the average variability calculated as the standard error of 3 measurements on each membrane was 0.2 %. The observation to be made from this information is that procedural error was very minor in comparison to the variability between different membranes. Detailed data for the repeated porosity experiments is located in Appendix III (Table A-3, Porosity Error Calculation Data).

2.3.3 Tortuosity

Tortuosity experiments were conducted with ^{14}C-labeled sucrose under very dilute conditions in de-ionized water. For all tests, the initial feed cell sucrose concentrations were approximately 2.0×10^{-8} M in 100 mL of feed solute (2.8×10^{4} dpm/mL), with an initial pH of 7, in the transport apparatus illustrated in Figure 2.2. Equation 2.5 (determining the effective diffusion coefficient through the membrane, D_{eff}) and Equation 2.3 were utilized to determine the tortuosity of the material. The infinite-dilution diffusion coefficient in water (D_o) has been determined experimentally to be 0.5228×10^{-5} cm^2/s at 25°C (Cussler 1997).

Figure 2.4 graphically illustrates the calculation (Equation 2.5) of the sucrose diffusion coefficient from transport data collected for experiment 1A. Based on these data from this single diffusion experiment the effective diffusion coefficient was calculated to be 1.03×10^{-6} (cm^2/s). The tortuosity for this experiment was determined from Equation 2.4 to be 1.26 (unitless). The average tortuosity of the four sucrose experiments was determined to be 1.30 ± 0.07 as summarized in Table 2.3. When comparing this result to referenced estimates, the average tortuosity is below the range specified for pores in an impermeable solid and slightly lower than the ideal spherical particle model (Equation 2.4) calculation made previously (Cussler 1997). All tortuosities were determined using the experimentally determined average porosity (determined using 2-isopropanol) of $24.9 \pm 5.2\%$ and the infinite-dilution diffusion coefficient calculated from Equation 2.6.

Table 2.3 – Summary of Tortuosity Data

Experiment	D_{eff} (cm^2/s 10^6)	Tortuosity
^{14}C-Labeled Sucrose		
Cell 1A	1.03	1.26
Cell 3A	1.00	1.30
Cell 5A	0.95	1.37
Cell 9A	1.03	1.26
Average	1.00 ± 0.7	1.30 ± 0.07

Figure 2.4 - Determination of Effective Diffusion Coefficient

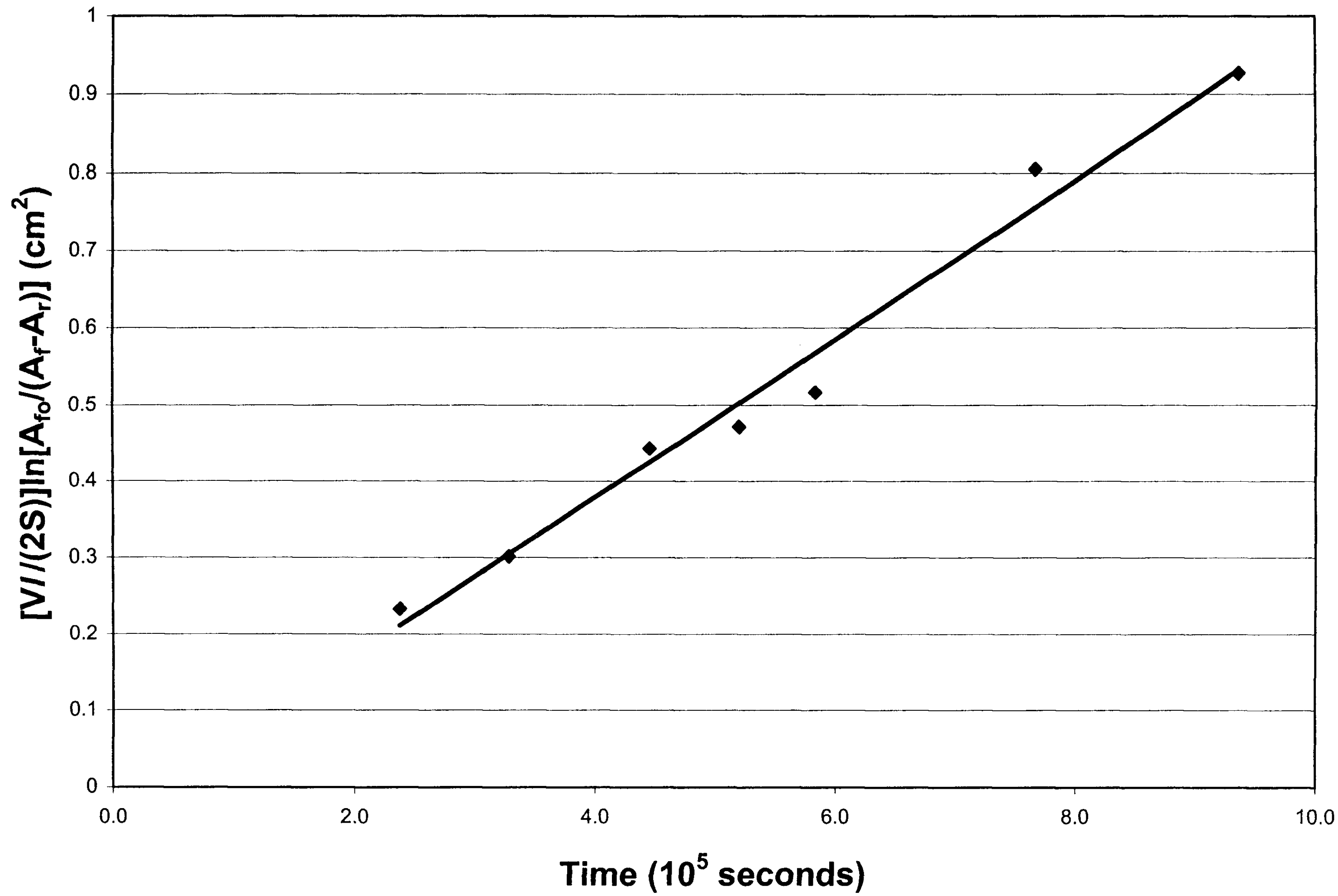

2.3.4 Optical Microscopy

Figure 2.5 shows an optical microscope photograph for a cross-section of a cleaned Mott® stainless steel membrane (magnified of by a factor 500). Using gray scale digital

Figure 2.5 – Mott® Stainless Steel Membrane Optical Microscopy

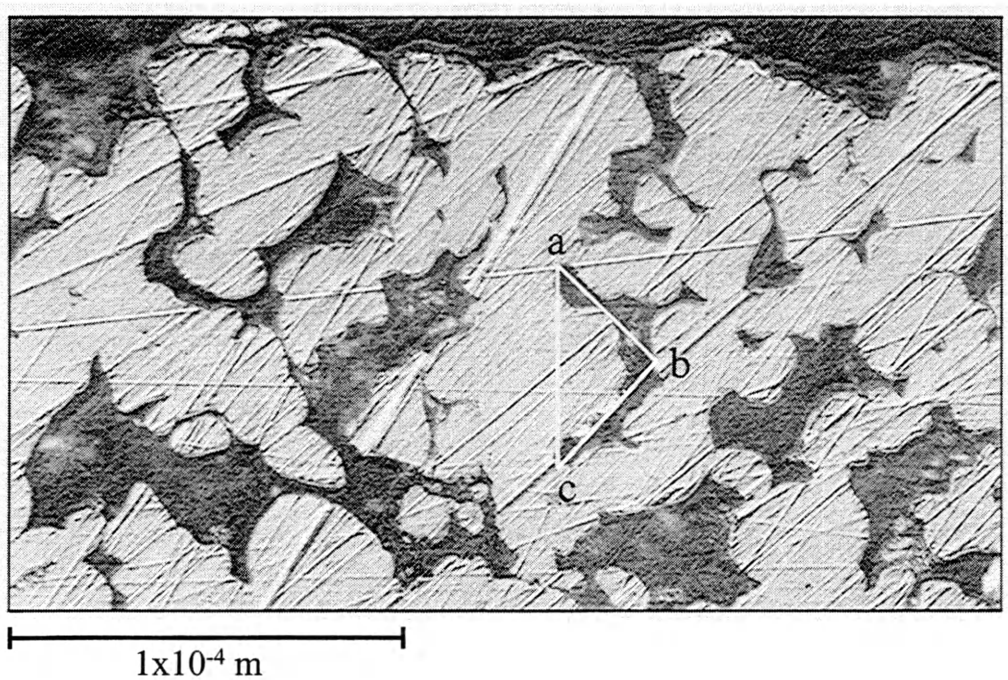

analysis (SCION™ 2000), an estimate of the porosity, pore diameter and the tortuosity was determined in two dimensions.

The porosity was determined by analyzing the area of dark gray relative to lighter gray and calculating a simple percentage. Figure 2.6 graphically illustrates the relative gray scale area for the membrane shown in Figure 2.5 with membrane void gray scale

Figure 2.6 - Porosity Optical Gray Scale Analysis

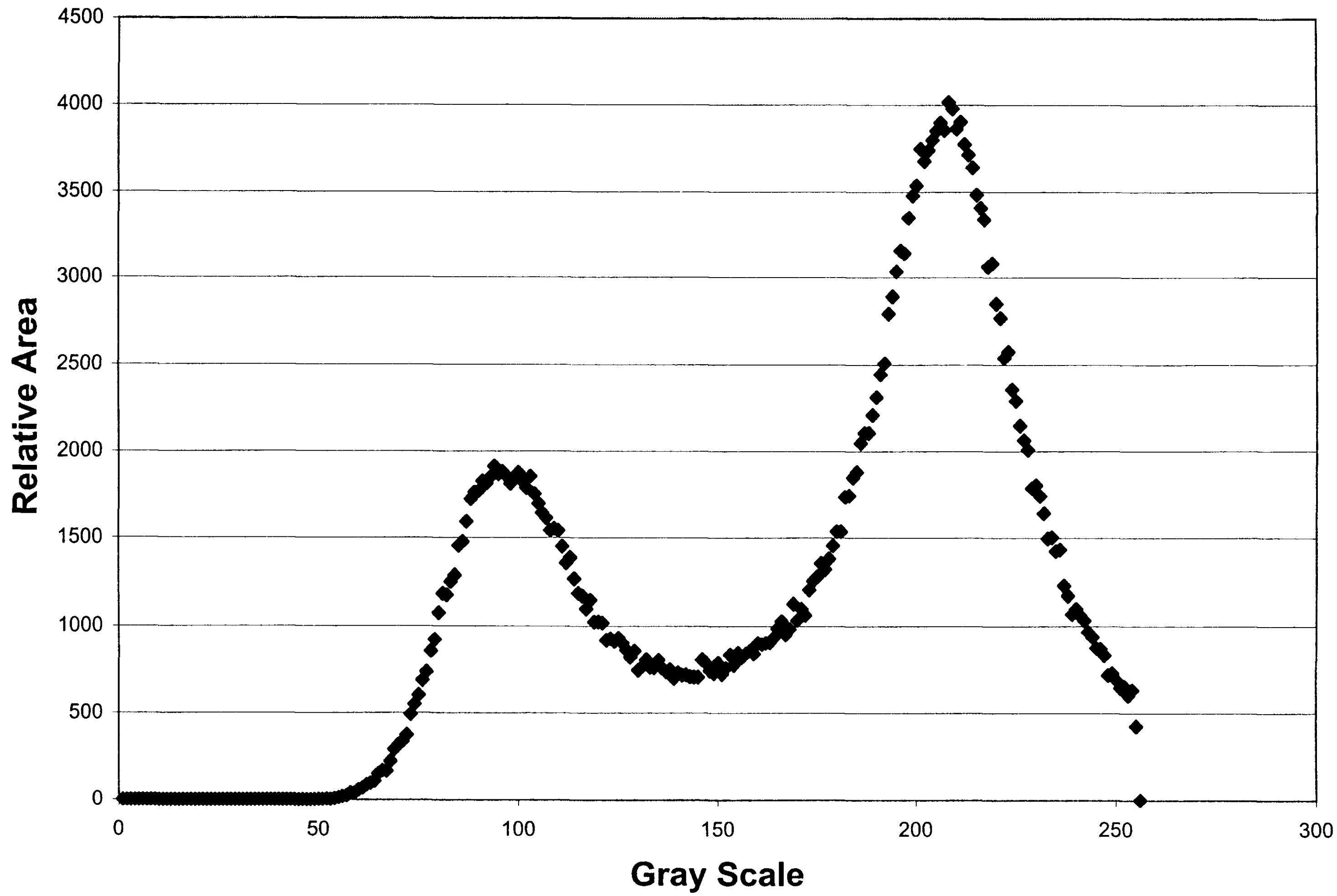

represented by the left peak and stainless steel material the right peak. The tortuosity was estimated by approximating the length of each void relative to the distance across the thickness of the membrane (for the example on Figure 2.5, line abc divided by line ac). The pore diameter could then be estimated as the total area of the void divided by the estimated total length of the pores for this membrane. Table 2.4 summarizes the results of the analysis using digitally scanned optical microscopy photographs and software entitled Scion Image provided by Scion® Corporation.

Table 2.4 – Digital Analysis Membrane Characteristics

Membrane Characteristic	Result
Porosity	27 %
Tortuosity	1.8
Pore Diameter (μm)	8

Worthy of note is that the porosity of this particular membrane determined digitally was estimated to be 27 % which is very consistent with that measured by the gravimetric techniques (24.9 %) described earlier. The estimate of pore diameter compares well to the more accurate experimental values reported above. Visual inspection of a cross-section of this material indicates that the tortuosity should not be significantly larger than unity (τ>1.0). The tortuosity calculated using the measured, or effective, diffusion coefficient, the experimentally determined porosity of 24.9 % and a known diffusion coefficient in dilute solution (Equation 2.3) was approximately 14 % larger than that estimated by visual inspection. Digital analysis membrane characteristics presented here are only estimates based on a two-dimensional analysis of a three-dimensional object and should be used for comparison to more accurate analytical techniques described above.

2.4 Summary and Conclusions

A significant amount of data were gathered during the characterization experiments performed at CSM. First, the membrane pore size distribution was measured using a gas flow porometry apparatus from which the relative flow through a given pore diameter can be determined. Next, membrane porosity data were generated from the simple mass difference between liquid saturated and dry membranes. Finally, tortuosities of the membrane were determined using a method that compares a measured effective diffusion coefficient and the known diffusion coefficient for sucrose. Results of the characterization experimentation are as follows:

- On the average, the mean pore diameter for these membranes was determined to be 2.2 ± 0.5 μm using 2-isopropanol as the test solvent. The stainless steel membranes exhibited a wide pore size distribution averaging between 1.2 and 3.7 μm also for experiments using 2-isopropanol as the test solvent.
- The average the porosity of 36 membranes tested was estimated to be 24.9 ± 5.2 % based on experimentation using 2-isopropanol as the test solvent. The variability in the porosity is considered large and is believed

to be a characteristic of the membrane material rather than porosity experimental procedure.

- An average tortuosity of 1.30 ± 0.07, which was below the tortuosity range of 3 to 6 specified in Cussler (1997) for pores in an impermeable solid and lower than the estimate for the ideal spherical particle model, was measured for four different stainless steel membranes using from ^{14}C-labeled sucrose as the diffusing solute.

The membrane characterization information detailed above has proven to be interesting in that the mean pore diameter calculated was determined to be consistent with the manufacturer's specified range, yet the pore size distribution seemed to be much larger than the manufacturers range of 2 to 3 μm. Also, results indicate that the stainless steel membrane has a significantly smaller porosity when compared to that estimated early in this study (40%) from alumina membrane characterization research (Bluhm 1999). And finally, the tortuosity determined from diffusion data, using dilute sucrose in water, compares well with estimates from reputable references.

Chapter 3 STAINLESS STEEL MEMBRANE TRANSPORT STUDIES

3.1 Introduction

The purpose of this portion of the investigation was to determine basic transport behavior of cations through the unmodified sintered stainless steel membranes as a function of pH. Transport behaviors were compared using characteristics such as effective diffusion coefficient (D_{eff}) which is defined as the diffusion coefficient of a solute over the length of a given medium. In the experimentation described in detail below, the medium is a water-saturated stainless steel membrane. The hypothesis was that, due to the large pore size of the stainless steel membranes examined diffusion was the rate controlling mechanism. Empirical tests were conducted to determine rates of diffusion of subject ions in a batch, small-scale test apparatus over appropriate time periods developed from initial diffusion rate data.

3.2 Experimental

Effective diffusion coefficients were determined using a relationship between the concentration (determined from radiotracer cation activity) in both the feed and permeate cells of a transport apparatus, as a function of time. The stainless steel membrane material was located in a bridge between the two cells. The stainless steel membrane material chosen for these studies was manufactured by Mott® Metal Corporation (Farmington, Connecticut) and is described by the manufacturer as a sintered 316 stainless steel membrane with pore diameter between 2 and 3 μm. The membrane thickness was measured to be between 0.123 cm and 0.124 cm with actual material used during experimentation and each membrane was cut from sheet material into disks measuring 25 mm in diameter.

3.2.1 Membrane Cleaning Process

Prior to testing, the membrane material was cleansed using a three-step process (Appendix I.1) which developed by Los Alamos personnel and used in the treatment of membranes prior to chemical modification. The procedure (Appendix I.1) consisted of solvent/oil removal by cleansing in an ozone generator for 20 minutes, etching the surface with 25% HCl for 5 minutes, and a de-ionized water (DI) wash in an ultrasonic cleanser for 24 hours.

3.2.2 Chemicals and Radiotracers

Similar investigations using alumina membranes determined effective diffusion coefficients for Fe^{3+}, Cs^{+}, Sr^{2+}, Ca^{2+}, Eu^{3+}, Am^{3+}, and Na^{+} in solutions of each metal salt (Bluhm 1999; Bluhm 2000). Comparable tests were conducted with the stainless steel membrane during this phase of experimentation and cations tested were determined based on the experienced recommendations of faculty at CSM and staff at LANL, and information obtained from applicable literature. To be specific, cations chosen for transport experimentation were based on charge (monovalent to tetravalent), on the desire to determine transport characteristics with cations that would be seen in the actual processing environment (actinides), and on results from recently completed alumina transport studies (Bluhm 1999; Bluhm 2000). Transport tests were conducted with Cs^+, Ca^{2+}, Eu^{3+}, Am^{3+}, and Pu^{4+} as radiotracers (^{45}Ca, ^{137}Cs, ^{241}Am, ^{152}Eu, and ^{239}Pu) in solutions with varying pH. Ranges for solution pH were 5-9 for cesium and calcium, 2-3.5 for americium, and 1-3 for plutonium. Europium transport experiments were only conducted at pH 2 as a limited amount of the radiotracer was available. Radiotracer concentrations varied between 10^{-7} and 10^{-12} M. Commercially available, reagent-grade chemicals were used in all experiments.

3.2.3 Transport Experimental Apparatus and Procedure

Each transport test was conducted in an apparatus consisting of Teflon® feed and permeate (receiver) transport cells (each approximately 250 mL in volume and cross-section diameter of 5 cm, filled with 100 mL of solution) joined by a bridge containing the stainless steel membrane disk. The bridge halves (also Teflon®) were threaded into each cell wall, sealed with Viton® 0-rings, and held in place with a circular clamp. The cells were covered with friction-seal Teflon® caps (which were not air-tight) to prevent evaporation.

After a cleaned membrane was obtained, the apparatus was cleaned and assembled. Prior to addition of the radiotracer and reagents, the apparatus was leak tested by filling both cells with the required volume of DI water and allowing the apparatus to stand for one day. If water leaks were observed, the apparatus was disassembled, repairs made and the cell again tested for leaks. Next, the nitrate ionic strength in both feed and permeate cells was adjusted to 0.001 M by adding a calculated amount of $NaNO_3$. Then each cell was adjusted to the desired pH with small volumes of dilute NaOH or HNO_3 using fine tip disposable pipettes. Finally, the calculated volume of radiotracer stock was added to the feed cell and the feed cell pH was again adjusted to the desired value. In total, less than 0.5 ml of the radio tracer stock and pH adjustment solutions were added to each cell prior to initiating a transport experiment. Samples were removed for analysis approximately every other day over the duration of each experiment with each sample ranging from 0.1 to 0.5 mL, depending on the activity of the radiotracer in solution. Transport rates were determined by determining the activity in each cell as a function of time. As samples were gathered, activities were measured by counting the sample on either a NaI gamma counter (Cs) or a liquid scintillation counter (Ca, Am, Pu and Eu). Solution pH was measured at the beginning and at the end of each experiment. Also, both feed and permeate cells of the apparatus were continuously mixed with a magnetic stirrer at a rate of 300 rpm.

Individual experimental testing periods ranged from 2 to 3 weeks. Standard procedures were developed and used to ensure repeatability in the cation transport experiments (Appendix I.2, Transport Experimental Procedure), as well as in assembling, sampling and cleaning of the transport apparatus during and after each experiment. Figure 3.1 provides an illustration of the transport apparatus and lists a summary of general test conditions.

3.2.4 Derivation of Effective Diffusion Coefficient (D_{eff})/Activity (A) Relationships

Preliminary transport characteristic comparisons were conducted by measuring the change of the radiotracer cation activity in both the receiver and feed cells as a function of time then calculating the effective diffusion coefficient as described by Cussler (1997).

Figure 3.1 – Transport Experimental Test Apparatus

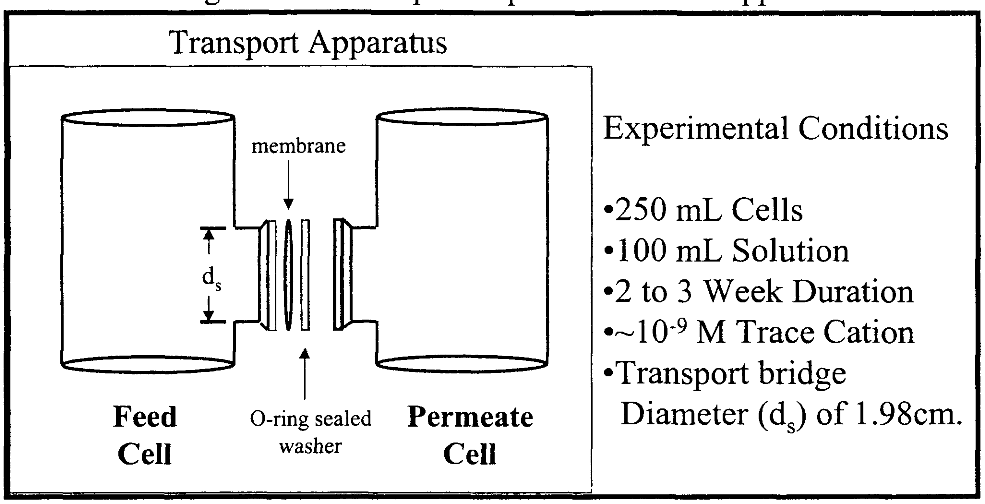

Using Fick's Law (Equation 3.1), the feed (Equation 3.9) and permeate cell mass balances, the membrane mass balance (Equation 3.2) and the driving force, a relationship is developed between the cation activity and the bulk, infinite-dilution diffusion coefficient (D) for both the feed side and the permeate side of the cell. Figure 3.2 illustrates the details of the membrane system and lists system variables. For this transport system, the effective diffusion coefficient (D_{eff}) is used in place of the bulk coefficient in order to compensate for possible transport resistances caused by the apparatus and membrane.

$$J = -D_{eff}\frac{dA}{dx} \qquad \text{Equation 3.1}$$

Where J = Cation flux (A/cm^2-s).
A = Activity (cpm).
D_{eff} = Cation effective diffusion coefficient (cm^2/s).
x = Distance across membrane (cm).

$$\frac{\partial A}{\partial t} + v_x\frac{\partial A}{\partial x} = D_{eff}\left(\frac{\partial^2 A}{\partial x^2}\right) \qquad \text{Equation 3.2}$$

Figure 3.2 - Porous Stainless Steel Membrane

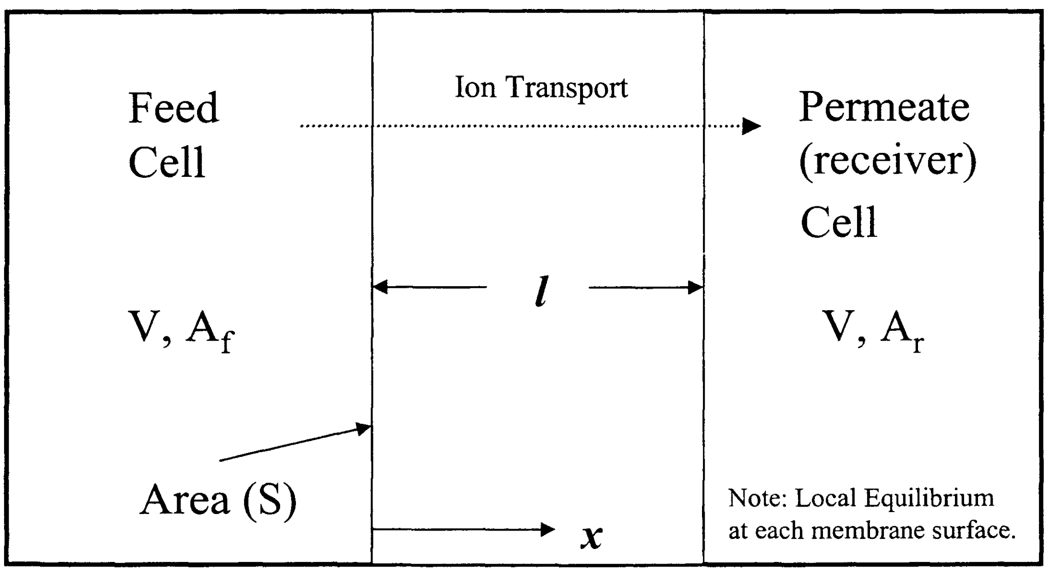

Where V = Volume of the feed or permeate side cell (cm^3).
S = Membrane surface area in contact with fluid (cm^2).
A_f = Activity (cpm) in the feed cell at time t (s).
A_r = Activity (cpm) in the permeate cell at time t (s).
A_{fo}= Activity (cpm) of the feed at t=0.
l = Membrane thickness (cm).

Because it is assumed that bulk convection is small in the x-direction (volumes in each cell are approximately equal), the mass velocity in the x-direction is insignificant and can be eliminated from the membrane mass balance (Equation 3.2). Since the change in activity in the membrane is very small compared to the activity in the total volume (both the feed and permeate cells) of the transport apparatus, the system can be assumed to be at a pseudo steady-state. Simply stated, the change in activity in the feed or permeate cells is considered extremely slow as compared to the effective diffusion of the cation through the membrane (i.e., there is no significant lag-time). As a result, the flux at the feed and permeate interfaces of the membrane are assumed to be equal (Equations 3.3 and 3.4).

$$J_{x=0} = J_{x=l}$$ Equation 3.3

$$\frac{dA_f}{dt} = \frac{dA_r}{dt} \quad or \quad dA_f = dA_r$$ Equation 3.4

Where $A_r = 0$ and $A_f = A_{fo}$ at t=0
$A_r = A_r$ and $A_f = A_f$ at t>0

It is also assumed that equilibrium is established at both the feed and permeate interfaces with the membrane, and that only the solute diffuses (no bulk flow) through the membrane. When Equation 3.4 is integrated, the result is the system overall mass balance (Equation 3.5).

$$A_{fo} - A_f = A_r$$ Equation 3.5

Assuming pseudo steady state and using Equation 3.2, a second order differential equation (Equation 3.6) is generated.

$$\frac{d^2 A}{dx^2} = 0 \qquad \text{Equation 3.6}$$

Where $A = A_f$ at x=0
$A = A_r$ at x=l

Integrating twice, given the boundary conditions of the membrane, results in a relationship between the activity and the distance into the membrane material (Equation 3.7).

$$A(x) = (\frac{A_r - A_f}{l})x + A_r \qquad \text{Equation 3.7}$$

Differentiating Equation 3.7 and substituting into Equation 3.1 results in Equation 3.8, the flux in terms of the activity driving force.

$$J(x) = -D_{eff} \frac{(A_r - A_f)}{l} \qquad \text{Equation 3.8}$$

Finally, an expression can then be developed for the activity in the feed cell as a function of time (as will be shown in Equations 3.11) from the general unsteady state mass balance for the feed cell (Equation 3.9).

$$-V \frac{\partial A_f}{\partial t} = SJ_{x=0} = SD_{eff} \frac{\partial A}{\partial x} \qquad \text{Equation 3.9}$$

The first derivative of the relationship between the activity as a function of the distance across the membrane (Equation 3.7) is substituted into Equation 3.9 which results in the following.

$$\frac{dA_f}{dt} = \frac{SD_{eff}}{Vl}(2A_f - A_{fo})$$ Equation 3.10

After separating variables and integrating over the boundary conditions, the equation is developed detailing the activity in the feed cell of the transport apparatus as a function of time (Equation 3.11).

$$A_f = \frac{1}{2}A_{fo}(1 + e^{-(\frac{2SD_{eff}t}{Vl})})$$ Equation 3.11

Similarly, for the permeate (receiving) cell, the relationship developed is given in Equation 3.12.

$$A_r = \frac{1}{2}A_{fo}(1 - e^{-(\frac{2SD_{eff}t}{Vl})})$$ Equation 3.12

At this point, the effective diffusion coefficient can be determined using either Equation 3.11 or 3.12. However, as discovered during analysis of experimental data, either of these two equations individually is very sensitive to small changes in activity in the membrane. To correct for this problem, the analysis is conducted with the difference of the two relationships as shown in Equation 3.13 (Cussler 1997).

$$A_f - A_r = \frac{1}{2}A_{fo}(1 + e^{-(\frac{2SD_{eff}t}{Vl})} - 1 + e^{-(\frac{2SD_{eff}t}{Vl})}) = A_{fo}(e^{-(\frac{2SD_{eff}t}{Vl})})$$ Equation 3.13

Equation 3.13 can be rearranged and written in a log-linear form as shown in Equation 3.14.

$$\frac{Vl}{2S}Ln(\frac{A_{fo}}{A_f - A_r}) = D_{eff}t$$ Equation 3.14

From this relationship, a least squares analysis of the data can be conducted to determine the effective diffusion coefficient (the slope of the best fit line) using feed and permeate cell activity data gathered over the duration of each experiment. Figure 3.3 illustrates the linear least squares regression method used to determine the effective diffusion coefficient for Cs transport data through a stainless steel membrane at an initial pH of 7.0 (run Cs5G). The effective diffusion coefficient for this example was determined to be 9.9×10^{-7} cm^2/s.

3.3 Results

The following section provides the details of cation transport experimental conditions, provides cation elemental data; attempts to explain test condition limitations, and lists a summary of results for each cation including the effective diffusion coefficient at test conditions.

3.3.1 Effective Diffusion Coefficients for Radiotracer Cations

Effective diffusion coefficients were determined experimentally as described in Section 3.2. Each experiment was performed with a new (and cleaned) stainless steel membrane with the exception of two sets of experiments where Cs transport tests were repeated once with the same membranes. Both the feed and permeate cells of a thoroughly cleaned apparatus were filled with 100 mL of distilled water (purified through a Milli-Q water purification system). For the Cs and Ca experiments, the ionic

Figure 3.3 - Determination of Effective Diffusion Coefficient For Cs at pH 7

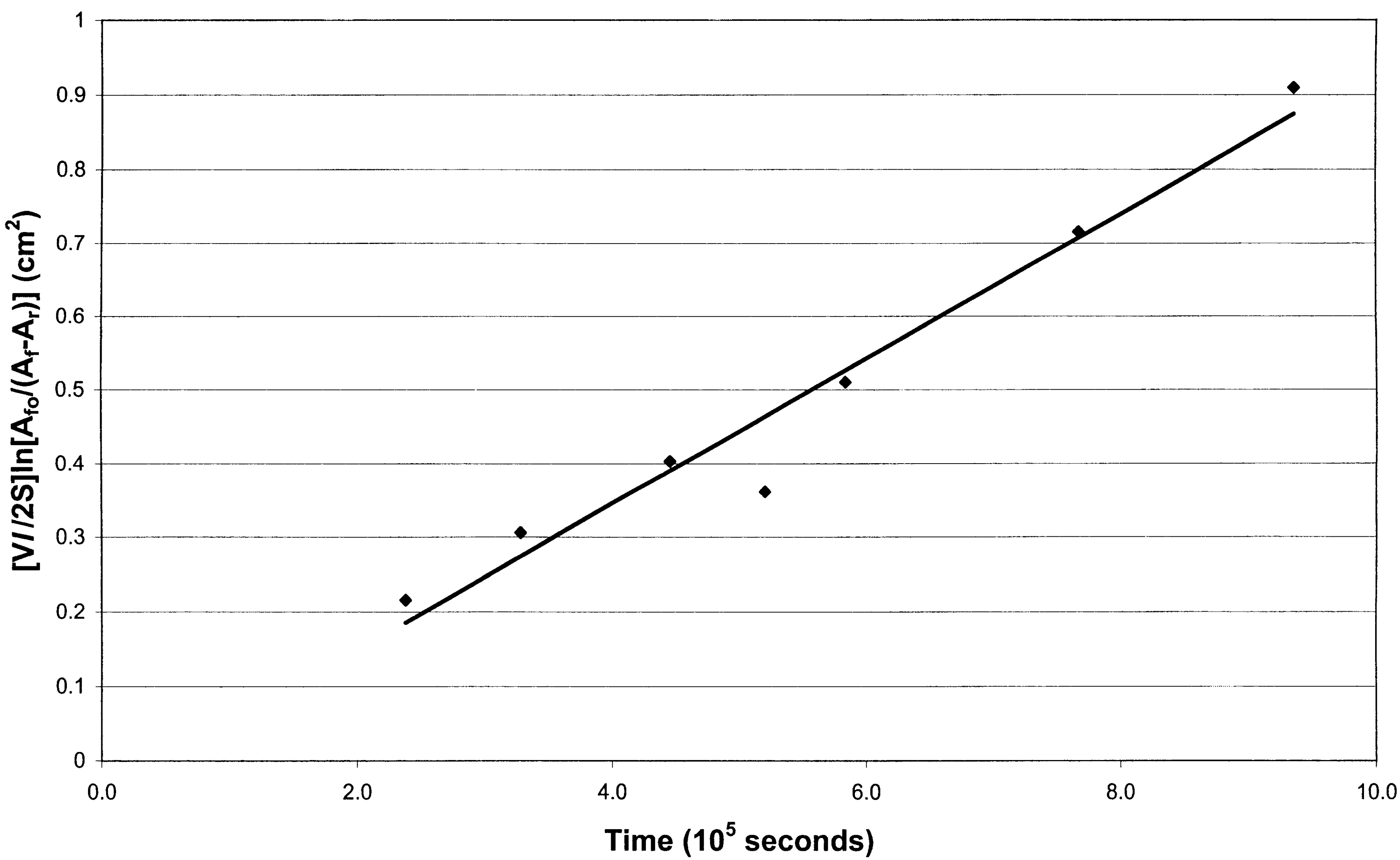

strength ($NaNO_3$) of the system was adjusted to 0.001 M with $NaNO_3$ so as to eliminate any variability caused by changes in ionic strength due to addition of the radiotracer (Bluhm 1999). The required concentration of the cation under investigation varied depending on the energy of the radioactivity being monitored. Table 3.1 lists the initial feed cell radiotracer concentration and activity for each set of transport experiments (Parrington 1996).

Table 3.1 – Radiotracer Activity Specifications

Cation	Radiotracer Cation Concentration (M)	Feed Cell Activity (counts/m-mL)	Radioactivity Monitored
^{45}Ca	2.50×10^{-11}	4.4×10^{5}	Beta
^{137}Cs	1.74×10^{-8}	2.8×10^{6}	Gamma
^{152}Eu	9.30×10^{-12}	9.8×10^{3}	Beta
^{241}Am	2.02×10^{-7}	1.1×10^{3}	Alpha
^{239}Pu	5.29×10^{-7}	1.8×10^{4}	Alpha

Table 3.2 provides a summary of the radiotracer cation effective diffusion coefficient results for each experiment, the average effective diffusion coefficient at each pH for a given cation, and the overall effective diffusion coefficient for each cation. As can be seen from the data, where the pH has been varied, a slight difference in the average effective diffusion coefficient is observed. However, these data are not statistically different, so the overall effective diffusion coefficient for all pHs is considered significant rather than each pH range for each cation. Statistical error is

Table 3.2 – Cation Effective Diffusion Coefficient Summary

Run Number	Initial pH	D_{eff} ($cm^2/s\ 10^7$)	R^2	Average D_{eff} ($cm^2/s\ 10^7$)	Average D_{eff} All pH ($cm^2/s\ 10^7$)	D_{eff} 95% Confidence Interval All pH ($cm^2/s\ 10^7$)
Cesium						
Cs5A	5	4.1	0.95	7.3	8.7	2.4
Cs1B	5	16	0.98			
Cs1C	5	5.2	1.00			
Cs9E	5	3.4	1.00			
Cs2B	7	6.4	0.98	9.0		
Cs2C	7	7.4	1.00			
Cs2D	7	16	1.00			
Cs6F	7	6.1	1.00			
Cs6G	7	6.9	1.00			
Cs1G	7	9.9	1.00			
Cs2G	7	6.7	1.00			
Cs3G	7	11	1.00			
Cs5G	7	9.9	0.96			
Cs9G	7	10	1.00			
Cs4A	9	18	0.97	9.1		
Cs3B	9	15	0.99			
Cs7F	9	3.4	1.00			
Cs7G	9	4.1	1.00			
Cs3C	9	4.6	0.96			
Calcium						
Ca4B	5	9.1	0.99	5.4	6.0	1.9
Ca1C	5	7.5	0.94			
Ca4D	5	3.6	0.98			
Ca4H	5	1.4	0.97			
Ca5B	7	7.3	0.93	5.2		
Ca5E	7	5.2	0.98			
Ca6G	7	2.9	0.91			
Ca3A	9	9.7	0.91	7.1		
Ca3F	9	5.9	0.91			
Ca6B	9	8.8	0.81			
Ca7G	9	4.1	0.93			
Europium						
Eu4A	2	6.2	0.98	4.9	4.9	3.6
Eu4B	2	4.0	1.00			
Eu1C	2	4.5	0.93			

Table 3.2 (cont.) – Cation Effective Diffusion Coefficient Summary

Run Number	Initial pH	D_{eff} ($cm^2/s\ 10^7$)	R^2	Average D_{eff} ($cm^2/s\ 10^7$)	Average D_{eff} All pH ($cm^2/s\ 10^7$)	D_{eff} 95% Confidence Interval All pH ($cm^2/s\ 10^7$)
Americium						
Am1A	2	6.3	0.93	6.0	6.0	1.6
Am9D	2	7.1	0.95			
Am4E	2	5.3	0.95			
Am1F	2	5.4	0.98			
Am2A	3.5	1.9	0.98	2.0	2.0	1.6
Am1E	3.5	0.80	0.88			
Am2E	3.5	3.3	0.97			
Plutonium[a]						
Pu1A	1	5.1	0.98	4.8	4.4	1.2
Pu4B	1	4.8	0.99			
Pu1C	1	4.0	0.97			
Pu1D	1	5.3	0.98			
Pu5B	2	4.2	1.00	4.3		
Pu2C	2	2.4	0.97			
Pu2D	2	5.1	1.00			
Pu3D	2	5.4	1.00			
Pu3A	3	0.52	0.97	4.0		
Pu6B	3	3.8	1.00			
Pu3C	3	4.0	0.94			
Pu9E	3	7.6	0.99			

[a]Plutonium determined to be present in solution as $Pu(OH)^{3+}$

reported for a 95% confidence interval (Moore 1989, Gorden 1972).

Figure 3.4 gives a composite illustration of the plutonium transport data developed at pH 1. The slope of each curve corresponds to an effective diffusion coefficient determined from data gathered during one transport experiment. For this example, each of the 4 runs resulted in similar slopes with the average D_{eff} determined to be $4.9x10^{-7}$ cm^2/s.

Figure 3.4 - Plutonium Transport Data pH 1

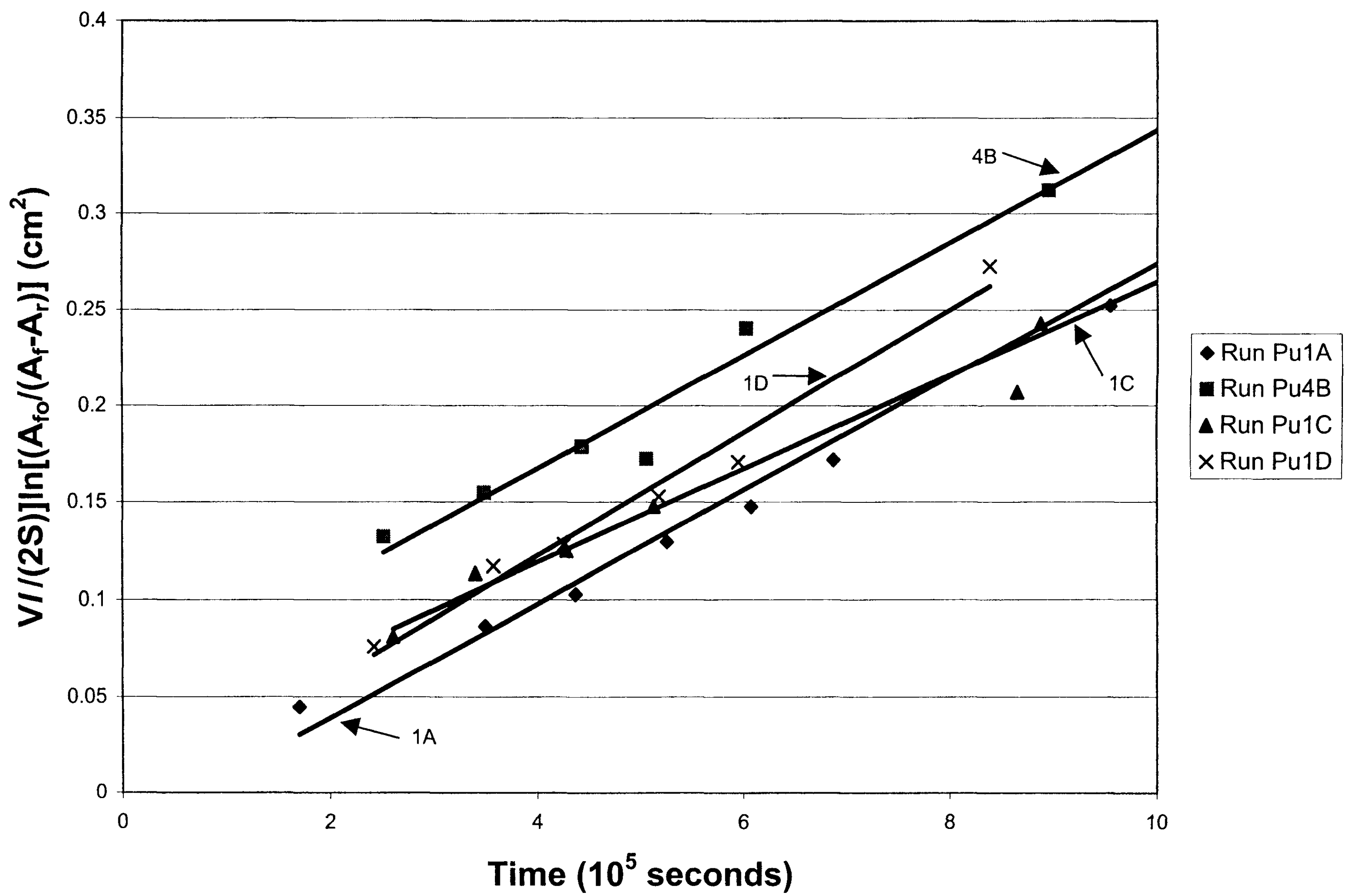

3.3.1.1 Cesium Transport

The transport experiments completed with ^{137}Cs as the radiotracer were conducted at very close to neutral conditions (at initial pH of 5, 7 and 9). Alkali metal hydroxides are strong bases, thus Cs^+ was considered to be completely dissociated under experimental conditions (Baes 1976). Experimental results for nineteen transport runs gave an average effective diffusion coefficient of $8.7 \times 10^{-7} \pm 2.4 \times 10^{-7}$ cm^2/s. Cesium proved to be the least difficult radiotracer cation with which to conduct experimentation as the cation has very high gamma energies (easy to count, no counter adjustment was required as with low alpha and beta emitters) and transport results were very consistent from run to run. Two of the Cs transport tests were replicated once each, reusing the membrane under the same radiotracer and reagent conditions; tests at pH 7 (runs 6F and 6G) and tests at pH 9 (runs 7F and 7G). All other experiments were conducted with a new membrane which was counted (to obtain mass balance data) following the experiment and discarded.

3.3.1.2 Calcium Transport

The transport experiments completed with ^{45}Ca as the radiotracer were also conducted under near neutral conditions (at initial pH of 5, 7 and 9). Given the low calcium concentration and the system pH, all calcium was determined to be in solution as the divalent metal ion. The concentration of $Ca(OH)^+$ (aq) was determined to be on the order of 10^{-17}M, given the stability constant (LogK=0.64) for the reaction of the divalent metal cation with a single hydroxide.

Cation transport experimental results from eleven experiments gave an average effective diffusion coefficient of $6.0 \times 10^{-7} \pm 1.9 \times 10^{-7}$ cm^2/s. Detailed Ca effective diffusion coefficient data are located in Table 3.2.

3.3.1.3 Americium Transport

The transport experiments completed with ^{241}Am as the radiotracer were conducted under acidic conditions (at initial pH of 2, 3.5 and 5). Experimental results for four experiments gave an average effective diffusion coefficient (at the initial pH of 2) of $6.0 \times 10^{-7} \pm 1.6 \times 10^{-7}$ cm^2/s at the initial pH of 2. The effective diffusion coefficient for pH 3.5 was approximately half that at pH 2 and no cation transport was evident at pH 5. The explanation for this phenomena is that as the hydroxide ion concentration increases (increase in pH), a higher percentage of the Am becomes an insoluble hydroxide, limiting or eliminating americium transport across the stainless steel membrane. At pH 2, all americium was assumed to be in solution as the trivalent metal ion (Am^{3+}) in that the concentration of $Am(OH)^+$ (10^{-12}M) was determined to be far below the total Am concentration, given the trivalent cation/hydroxide reaction stability constant (LogK=6.9).

3.3.1.4 Plutonium Transport

Transport experiments completed with ^{239}Pu as the radiotracer were conducted in acidic conditions (at initial pH of 1, 2 and 3). Experimentation above pH 3 was avoided as hydrolysis begins to precipitate Pu from solution at these slightly acidic and at caustic conditions. However, when researching stability constants for the hydrolysis of plutonium, it was discovered that even in these highly acidic conditions, a single hydroxide is associated with Pu^{4+} (Baes 1976, Smith et al. 1997). In addition, at the Pu concentrations (~10^{-8} M) for our system, additional hydrolysis does not occur below pH 3 and precipitation of the colloidal Pu hydroxide does not occur below pH 7.5 (Cleveland 1979). Given this information, it was then assumed that all experimentation was conducted with plutonium as $Pu(OH)^{3+}$.

Experimental results for the twelve transport runs gave an average effective diffusion coefficient of $4.4 \times 10^{-7} \pm 1.2 \times 10^{-7}$ cm^2/s. Table 3.2 lists all detailed effective diffusion coefficient data for Pu experiments at pH 1, 2 and 3. Figure 3.4 illustrates the determination of diffusion coefficients for plutonium at pH 1.

3.3.1.5 Europium Transport

Transport experiments completed with ^{152}Eu as the radiotracer were conducted at only one pH (at initial pH of 2) because of a limited amount of the material. Given the extremely small cation concentration, the system pH and the stability constant (Log K= 5.42) for the trivalent cation/monohydroxide reaction, it was determined that all Eu was present in solution as the trivalent cation. Experimental results for the three experiments gave an average effective diffusion coefficient of $4.9 \times 10^{-7} \pm 3.6 \times 10^{-7}$ cm^2/s.

3.4 Discussion

The purpose of the discussion of the results is to explain trends and observations gathered during experimentation.

3.4.1 Comparison of Experimental and Referenced Infinite-dilution Diffusion Coefficients

Using Equation 2.3 (calculation of tortuosity from diffusion coefficients) and the experimentally determined tortuosity (1.3 ± 0.07) and porosity determined using 2-isopropanol (24.9 ± 5.2 %) detailed in Chapter 2, Stainless Steel Membrane Characterization, the experimental molecular or infinite-dilution diffusion coefficient (D_0) can be estimated. In Table 3.3, these estimates are presented and include the propagation of variability associated with the tortuosity, porosity and the experimental effective diffusion coefficient (D_{eff}) using a standard propagation of error analysis (Moore 1989, Gordon 1972). Table 3.3 also includes bulk infinite-dilution diffusion coefficients found in literature for all cations with the exception of plutonium (not available in the industry at this time).

Table 3.3 – Comparison of Experimental D_0 and D_0 from Referenced Literature

Cation	Average Experimental D_{eff} (cm^2/s 10^7)	D_0 From Literature (cm^2/s 10^6)	Experimental D_0 (cm^2/s 10^6)	Difference (%)
Cs^+,	8.7 ± 2.4	10.0[a]	4.6 ± 1.6	38
Ca^{2+}	6.0 ± 1.9	7.9[b]	3.1 ± 1.2	46
Eu^{3+}	4.9 ± 3.6	5.18[c]	2.5 ± 1.9	15
Am^{3+}	6.0 ± 1.6	6.25[d]	3.1 ± 1.1	33
$Pu(OH)^{3+}$	4.4 ± 1.2	N/A	2.3 ± 0.8	N/A

[a]Harris 1997.
[b]Cussler 1997.
[a]Latrous 1982.
[b]Fourest 1984.

Results indicate that the infinite-dilution diffusion coefficients from referenced literature are higher than the range calculated for each cation experimental infinite-dilution diffusion coefficient (determined from D_{eff}) as indicated in Table 3.3. Low experimentally determined infinite-dilution diffusion coefficients are likely a result of the smaller than expected area for diffusion due to air trapped in the membrane pores as explained in Section 3.4.2.2.

3.4.2 Statistical Error of Effective Diffusion Coefficients

The statistical error (for the 95 % confidence interval) was determined for each cation overall effective diffusion coefficient. With the exception of Eu, errors ranged from 27 % for Pu to 32 % for Ca calculated from the 95% confidence interval. Europium effective diffusion coefficient error was higher (74 %) predominantly because only 3 experiments were conducted and the variability was larger.

An attempt was made to determine causes of error and identify physical inconsistencies in membrane material, the possibility of air trapped in membrane pores, and mass flow in the initial days of transport experiments due to differences in cell solution volumes. The purpose of this section is to identify and discuss possible sources of error.

3.4.2.1 Repeatability of Experiments

Each experiment was performed with a new (and cleaned) stainless steel membrane with the exception of two repeat experiments. Cesium transport experiments were repeated, without drying the membranes between runs, with runs 6F and 7F under identical conditions. As detailed in Table 3.4, the changes in effective diffusion coefficient were less than the calculated error determined for experiments where a new/cleaned membrane was used (Table 3.2). Even then, the data indicate that significant error still exists. Possible sources of errors not involving the membrane are differences in initial solution volume in the feed and permeate cells causing bulk flow, inconsistent sampling techniques, or errors caused by volume changes from sample removal.

Table 3.4 – Repeated Transport Experiments
(Reuse of Membrane)

Experiment	pH	D_{eff} ($cm^2/s\ 10^7$)	Curve Fit (R^2)	Difference in D_{eff} Between Runs (%)
Cs6F	7	6.1	1.00	-
Cs6G	7	6.9	1.00	12
Cs7F	9	3.4	1.00	-
Cs7G	9	4.1	1.00	17

3.4.2.2 Error Caused by Air in Stainless Steel Membrane Pores

Prior to initiating a transport experiment, the assembled apparatus was filled with DI water and tested for leaks for one day. Following this, the radiotracer stock solution was added to the feed cell and the transport experiment started. Other than the leak test/presoak step, no steps were taken to guarantee that all solution or gases in the membrane were replaced with water. A concern was expressed that a small volume of air might remain in the membrane essentially reducing the pore volume available for transport (reducing the porosity). As a result of this concern, a qualitative experiment was conducted to determine if air could still exist in the stainless steel membrane pores even after the membrane had been submerged in water (DI) for a significant period of time. In preparation for the test, two Mott® stainless steel membranes were soaked in DI water (water which was not degassed) for one day. The two membranes, remaining in water, were introduced into a vacuum chamber and the pressure was slowly reduced. Small bubbles (approximately 1 mm in diameter) began to appear on the stainless steel membrane at 520 torr, and the number increased until approximately 420 torr, eventually covering 5 to10 % of the membrane surface and suggesting the presence of significant air in the membrane pores. However, since the water was not degassed prior to the experiment, it is impossible to know how much air came from the membrane pores and how much came from the water.

As a consequence of the results above, a set of three Cs transport experiments (pH 7) were conducted with membranes saturated with DI water after saturating the membrane with a low surface tension, water-soluble solution, thus removing a high percentage of the air trapped in the membrane. In order to remove the air, the three membranes were submerged in 2-isopropanol for three days, installed in a transport cell, where 200 mL of DI water was then gravity fed through the membrane to remove the water-miscible solution.

As can be seen from the results listed in Table 3.5, the average D_{eff} nearly doubled as compared results from tests using membranes soaked only in water ($8.7x10^{-7}$ cm^2/s).

Table 3.5 – Comparison of Experimental D_0 and D_0 from Referenced Literature for Cs

Run	Average Experimental D_{eff} ($cm^2/s\ 10^6$)	D_0 From Literature ($cm^2/s\ 10^6$)	Experimental D_0 ($cm^2/s\ 10^6$)
Cs1H	1.70		8.8
Cs3H	1.74		9.0
Cs9H	1.63		8.4
Average	1.69 ± 0.16	10	8.8 ± 2.1

Also, the D_o from referenced literature falls well within the error range for the calculated D_o. The conclusion drawn from the above analysis was that the D_o calculated from the transport experiments conducted with membranes soaked only in DI water were calculated with an inappropriate porosity (porosity determined for membranes soaked in 2-isopropanol where the air had been removed). For the transport experiments where water saturated membranes were used, the porosity determined with membranes soaked in only DI water was more appropriate. The infinite-dilution diffusion coefficients were then recalculated using the porosity of water saturated stainless steel membranes (detailed in Section 2.3.2) determined to be 17.0 ± 4.8 %. Table 3.6 lists the recalculated experimental infinite-dilution diffusion coefficients and the coefficients found in referenced literature. Again note that the infinite-dilution diffusion coefficients (D_0) in Tables 3.5 and 3.6 were calculated using a tortuosity value determined using sucrose transport experiments which also may have used partially saturated membranes.

Table 3.6 - Corrected Experimental Summary for D_0

Cation	D_0 From Literature ($cm^2/s\ 10^6$)	Experimental D_0 ($cm^2/s\ 10^6$)
Cs^+,	10.0	7.0 ± 2.6^a
Ca^{2+}	7.9	4.5 ± 2.0
Eu^{3+}	5.18	3.7 ± 2.9
Am^{3+}	6.25	4.5 ± 1.8
$Pu(OH)^{3+}$	N/A	3.3 ± 1.3

[a]Includes runs Cs1H, Cs3H and Cs9H.

Conclusions from this analysis were that there was a substantial volume of air which remained in the DI water soaked stainless steel membranes (approximately 8 % by volume). This air contributed to the error and biased the effective diffusion coefficients below that which would have been determined otherwise. However, when recalculating the experimental infinite-dilution diffusion coefficient using the effective porosity determined for water soaked membranes, infinite-dilution diffusion coefficients from referenced literature fall within the range calculated for the experimental coefficient (Eu and Am), or are slightly higher than the experimental coefficient (Cs and Ca). This information strongly supports the hypothesis that diffusion is the rate controlling mechanism of solutes for these stainless steel membranes.

3.4.2.3 Mass Flow Due to Differences in Cell Head

When initiating a transport experiment, both the feed and receiver cells were filled with 99 mL of water (DI) and 1 mL of 0.1 M $NaNO_3$ solution. The cells were then placed aside for one day to test for leaks. Then the cells pH was adjusted with very small amounts of NaOH or HNO_3, as needed, using a fine tip pipette (μL droplets). Next, the acidic stock radiotracer solution, volumes ranging from 0.06 to 0.3 mL, was added to the feed cell. Finally, the feed cell pH was again adjusted to the correct pH. As a result of this procedure and volumetric measurement device error (graduated cylinder), it was evident that a small difference in hydraulic head existed between cells at the start of each transport experiment. Estimations were that the difference in head between the cells could have been caused by as much as a few percent difference in volume, causing bulk flow through the membrane during the early hours of each transport experiment. To estimate the approximate time period during which bulk flow of the solution (resulting from the hydrostatic pressure) existed, an analysis was conducted in order to determine how the hydraulic head decreased as a function of time. Figure 3.5 illustrates the system configuration for the derivation.

Initially, the system modeled as two tanks (feed and permeate cells) separated by a bundle of parallel of straight pipes which represented the pores in the porous stainless steel membrane. The energy balance for the system was determined from the Bernouli equation (Equation 3.15).

Figure 3.5 - Transport Apparatus

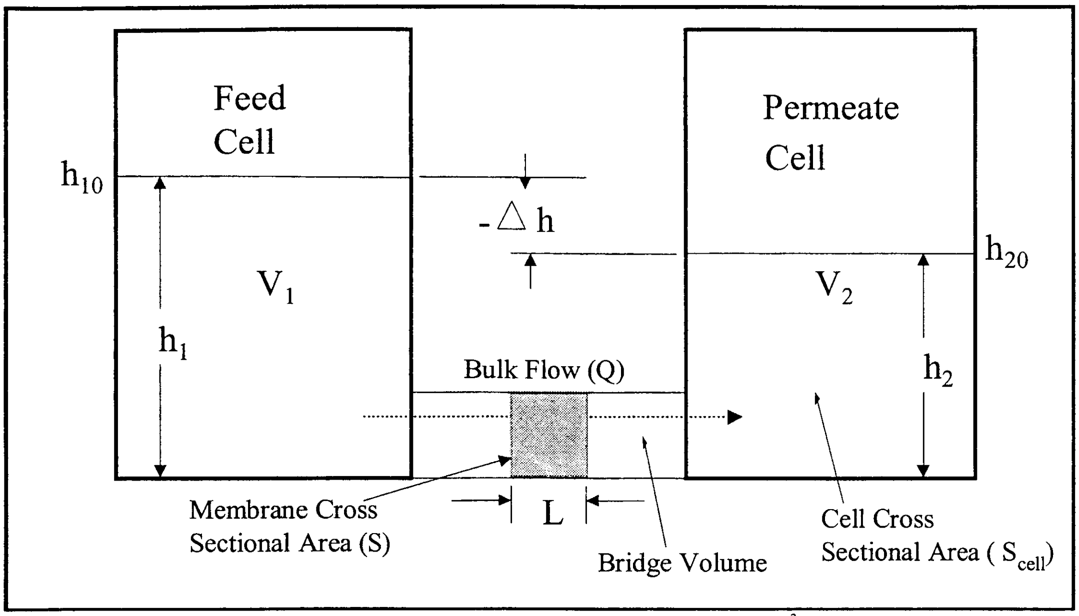

Where V = Volume of the feed or permeate side cell (cm^3).
S = Surface area available for transport (cm^2).
h = Height of feed (1) or permeate (2) cell liquid (cm).
L = Thickness or membrane (cm).
Q = Average bulk flow (cm^3/s).
S_{cell} = Cell Cross sectional area (cm^2).

$$g\Delta h + 2\langle v\rangle^2 \frac{L}{D} fN = 0 \qquad \text{Equation 3.15}$$

Where g = gravitational constant (cm/s^2).
f = Friction factor (unitless).
$\langle v\rangle$ = Average velocity of bulk flow in a pore (s).
D = Diameter of a pore, (cm).
N = Number of pipes in bundle

The volumetric flow rate (Q) and the average velocity are related by the transport cell cross-sectional area (S) as given by Equation 3.16.

$$Q = \langle v\rangle S \qquad \text{Equation 3.16}$$

For laminar flow, the friction factor (*f*) is proportional to the inverse of the average velocity, which combined with Equation 3.16 and simplified gives Equation 3.17. In order to simplify the equation, all constants were combined into one constant (K).

$$Q = -K\Delta h \qquad \text{Equation 3.17}$$

The constant, K, was then determined as follows. A single cell was filled with 150 mL of DI water and the other cell was disconnected with the membrane remaining in the bridge section of the apparatus. With no head pressure on the permeate side of the cell, 100 mL of water passed through the membrane in 51 hours. To determine K, these results were analyzed using the differential mass balance on the feed cell (Equation 3.18).

$$\frac{dV_1}{dt} = S_{cell}\frac{dh_1}{dt} = -Q = -K\Delta h \qquad \text{Equation 3.18}$$

Where S_{cell} = Cross-sectional area of transport cell (cm^2).

When Equation 3.18 is integrated using the initial fluid height, the result is Equation 3.19.

$$h_1 = h_{10}\exp\left(\frac{-Kt}{S_{cell}}\right) \qquad \text{Equation 3.19}$$

The time-average flow rate through the first period t is then described by Equation 3.20.

$$\langle Q\rangle = \frac{1}{t}\int_o^t Kh_1 d\hat{t} = \frac{1}{t}\int_o^t Kh_{10}\exp\left(\frac{-Kt}{S_{cell}}\right)dt = \frac{h_{10}K}{t}\left(1-\exp\left(\frac{-Kt}{S_{cell}}\right)\right) \qquad \text{Equation 3.20}$$

Where $\langle Q \rangle$ = Time averaged flow rate (mL/hr).
h_{10} = The initial height of the feed cell.

Equation 3.20 can then be written in terms of K and the initial and final volumes (V_{10} and V_{1f}) as shown in Equation 3.21.

$$K = -\frac{S_{cell}}{t}\ln\left(1-\frac{\left(V_{10}-V_{1f}\right)}{V_{10}}\right) \qquad \text{Equation 3.21}$$

Substituting data from experimentation into Equation 3.21, K was determined to be 0.0141 cm^2-hr^{-1}.

Since by mass balance the change in volume in the feed cell (Figure 3.5) is equal and opposite to that of the permeate cell (dV_1=-dV_2), and since S_{cell} is identical for both cells, we can conclude that Equation 3.22 is valid.

$$h_2 = h_{10} + h_{20} - h_1 \qquad \text{Equation 3.22}$$

Where h_{10} = The initial height of the feed cell.
H_{20} = The initial height of the permeate cell.

Using Equations 3.21, 3.22 and the initial transport apparatus conditions, the relationship between feed cell height and time was determined (Equation 3.23).

$$t = -\frac{S_{cell}}{2K}Ln\left[\frac{h_1-\frac{(h_{10}+h_{20})}{2}}{h_{10}-\frac{(h_{10}+h_{20})}{2}}\right] \qquad \text{Equation 3.23}$$

The ultimate goal of this derivation was to determine an estimate of the time needed for bulk flow to dissipate. The approach finally used was to estimate the time required for the head to fall to a given fraction of the initial hydraulic head (F, Equation 3.24).

$$F = \frac{h_1 - h_2}{h_{10} - h_{20}}$$ Equation 3.24

The final result, after substituting equation 3.24 into Equation 3.23 and simplifying, was the simple relationship described by Equation 3.25 and illustrated in Figure 3.6.

$$t = -35.6Ln(F)$$ Equation 3.25

Where t = Time for head to fall to fraction of the original head (hr).

The above derivation verified that mass flow will occur when a hydraulic head exists between transport cells.

We can also estimate the ratio of the bulk flux (J_{bulk}) to cation diffusion flux (J_{diff}) given the fundamental definitions of shown in Equations 3.26 and 3.27, respectively.

$$J_{Bulk} = c\langle v \rangle = \frac{cQ}{S} = \frac{cK\Delta h}{S} = \frac{cK\Delta V}{(S)S_{cell}}$$ Equation 3.25

Where $\langle v \rangle$ = Time averaged velocity.
Δh = The differential head between cells.
ΔV = The differential volume between cells.
c = Cation concentration.

$$J_{diff} = \frac{Dc}{L}$$ Equation 3.26

Where D = Cation diffusion coefficient.

Figure 3.6 - Fraction of Initial Head as a Function of Time

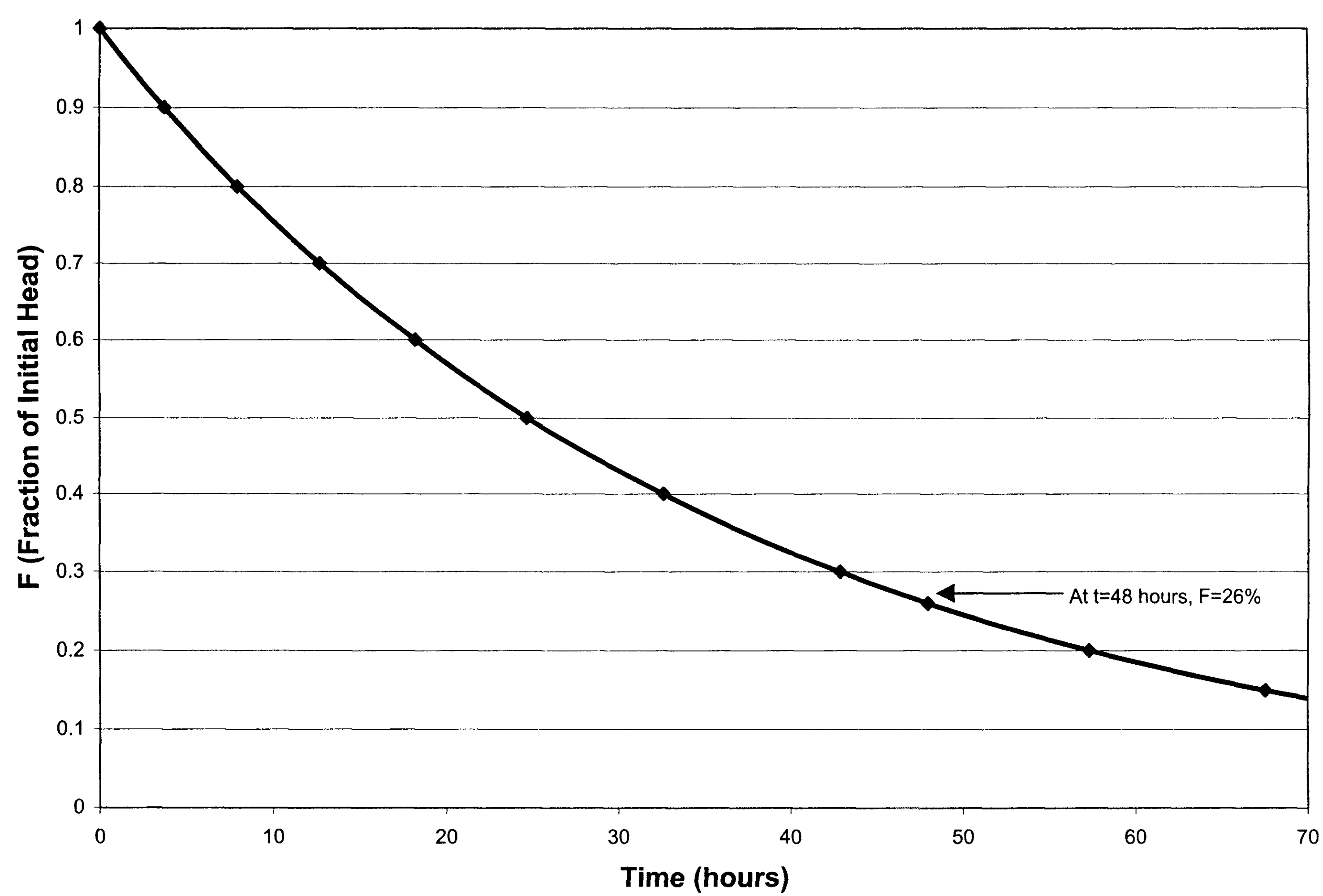

Dividing Equation 3.25 by 3.26 gives the ratio shown in Equation 3.27.

$$\frac{J_{Bulk}}{J_{Diff}} = \frac{LK\Delta V}{D(S)S_{cell}} \qquad \text{Equation 3.27}$$

Using membrane characteristic values determined previously, and a diffusion coefficient (D) value of $1\text{x}10^{-7}$ cm^2/s, and using Equation 3.27, it was determined that in order for the cation flux from bulk flow to be less than 10% that of the flux from diffusion, the differential volume would need to be less than 0.250mL. This estimate validates the concern over the impact of bulk flow on experimentally determining diffusion coefficients due to cell volume differences.

Given the likelihood that a few percent difference in volume did exist between the cells and influenced transport data, the decision was made that data gathered during the first 48 hours of experimentation would not be used in radiotracer cation effective diffusion coefficient determination. This time period was sufficient to reduce the head to approximately 26% of the initial height (using Equation 3.25) and to minimize effects due to volume differences of the magnitude expected. However, after the elimination of the first two days of transport data from the data analysis, the recalculated effective diffusion coefficients were not significantly (statistically) different than those calculated when including the first 48 hours of transport experimentation (listed in Table 3.2). These results infer that small differences in initial volume between transport cells do not significantly influence the outcome of the overall diffusion coefficients for our system given the current configuration.

3.4.2.4 Mass Balance Error

A complete mass balance of the radiotracer cation transport system could only be conducted for the Cs as the radioactivity monitored (gamma) was not shielded by the membrane material and did not prevent determining the Cs in tested membranes. With all other cation experiments, accurate measurements of the quantity of each cation in the tested membrane material was not possible. Following a Cs transport experiment we determined the amount of material in the membrane, the material in both the feed and permeate cells, and the sum of all samples taken. This final sum was then compared to the material initially in the feed cell. When examining all Cs experiments where membranes were counted following transport tests (12 experiments total), the average mass balance closed to within 9 ± 2 %. There are two possible contributions as to the variance in the mass balance. First, very small samples (8 to 10, 0.1 to 0.5 mL samples) were removed, but not replaced, from apparatus cells in order to minimize the change in volume for the purpose of maintaining a constant concentration driving force. The statistical variability (in the pipetting and gamma counting instruments) increases as smaller and smaller sample volumes are used to represent a large volume. After further consideration, it is believed to be highly likely that larger sample volumes at less frequent intervals would have reduced mass balance error.

Second, although many solution samples were removed by only one individual, some experiments were sampled by up to 3 different personnel. It is very possible that pipetting techniques differed between individuals resulting in different sample volumes. As a result, the variability in pipetting technique was considered to make an important contribution to the mass balance error.

An important observation seen while conducting cesium mass balances was that the amount of Cs determined to be in the membrane after completion of experimentation did not prove to be significant (less than 0.6 %) when computing the overall system mass balance.

3.4.3 Electrostatic (Membrane) Wall Effects on Effective diffusion

In an ionic solution, as the ions flow along the charged surface of an ionic membrane, mobile ions will flow along a surface of less mobile ions (also known as the double layer or shear plane). The electrical potential at this shear plane, the zeta potential (ζ), can be calculated from streaming potential measurements using the Helmholtz-Smoluchowski equation (Equation 3.28) (Mulder 1998; Schmid 1998). At a given ionic strength, the electrical potential is measured as a function of the solution applied pressure. The zeta potential is then obtained from the slope of the electrical potential-pressure plot.

The distance from the membrane surface to the shear plane can be estimated by the Debye length which can be calculated from the total ion concentration and ionic valance using Equation 3.29 (Schaep 1999).

$$\frac{\Delta\phi}{\Delta P} = \frac{\varepsilon\zeta}{\eta\kappa}$$ Equation 3.28

Where $\Delta\phi/\Delta P$ = Streaming potential (V/Pa).
ε = Dielectric Constant (C^2/Nm^2).
ζ = Zeta Potential (V).
η = Viscosity of the Solution(Pa-s).
κ = Electrical Conductivity of the Solution (Ω^{-1} -m^{-1}).

The Debye length (or double layer thickness) for the conditions of the transport experiments outlined in this document is estimated to be approximately $5.0\text{x}10^{-3}$ μm (0.001 M $NaNO_3$ for pH 3.0).

$$\lambda_D = (\frac{\varepsilon_0\varepsilon_r RT}{F^2\sum_i z_i^2 c_i})$$ Equation 3.29

Where λ_D= Debye length (m).
ε_0= Permittivity of vacuum (8.85E-12C V^{-1} -m^{-1}).
ε_r= Relative permittivity (78.3 for water at 25°C).
R= Universal gas constant (8.3143 J mol^{-1} -K^{-1}).
T= Temperature (K).
z_i= Valence of ion.
c_i= Ion concentration (mol-m^{-3}).

Given the experimentally determined mean pore diameter for the stainless steel membrane (2 μm) and using the Debye length calculated above, the pore diameter is calculated to be a factor of 400 larger than the Debye length. In addition, one key assumption of the Helmholtz-Smoluchowski equation is that pore diameter is greater than several hundred times the diameter of the diffusing molecule or it is assumed that wall effects do not have a significant influence on ionic species in solution. In the case of the stainless steel membranes, the ratio of the diameter of the largest molecule (calcium with a hydrated molecular radius of 6.0×10^{-4} μm, Table 3.2) under investigation to the pore diameter determined for the Mott® membrane is estimated to be 1700. Therefore, it was assumed that wall effects due to electrochemical conditions of the stainless steel membrane transport experiments were not significant.

3.4.4 Influence of Cation Size on Effective Diffusion Coefficient

Ideally, cation effective diffusion coefficients should decrease as the hydrated ionic radius of the cation increases, as shown by the Stokes-Einstein Equation (Equation 3.30) (Cussler 1997). However, results from the stainless steel effective diffusion studies indicate no statistical difference in effective diffusion coefficients for those ions with known hydrated radii. Nevertheless, a general trend can be seen as illustrated in Figure 3.7, which compares the mean effective diffusion coefficient for the cations with the values of the hydrated radius from references (Table 3.7). The trend is consistent with observations from references as there is a general decrease in diffusion coefficient with increasing ion radius (Harris 1991).

$$D = \frac{k_B T}{6\pi\mu R_0} \qquad \text{Equation 3.30}$$

Where k_B = Boltsmann's constant.
T = Temperature(K).
μ = Solvent viscosity.
R_0 = Solute radius.

Figure 3.7 - Effective Diffusion Coefficient as a Function of Solute Radius

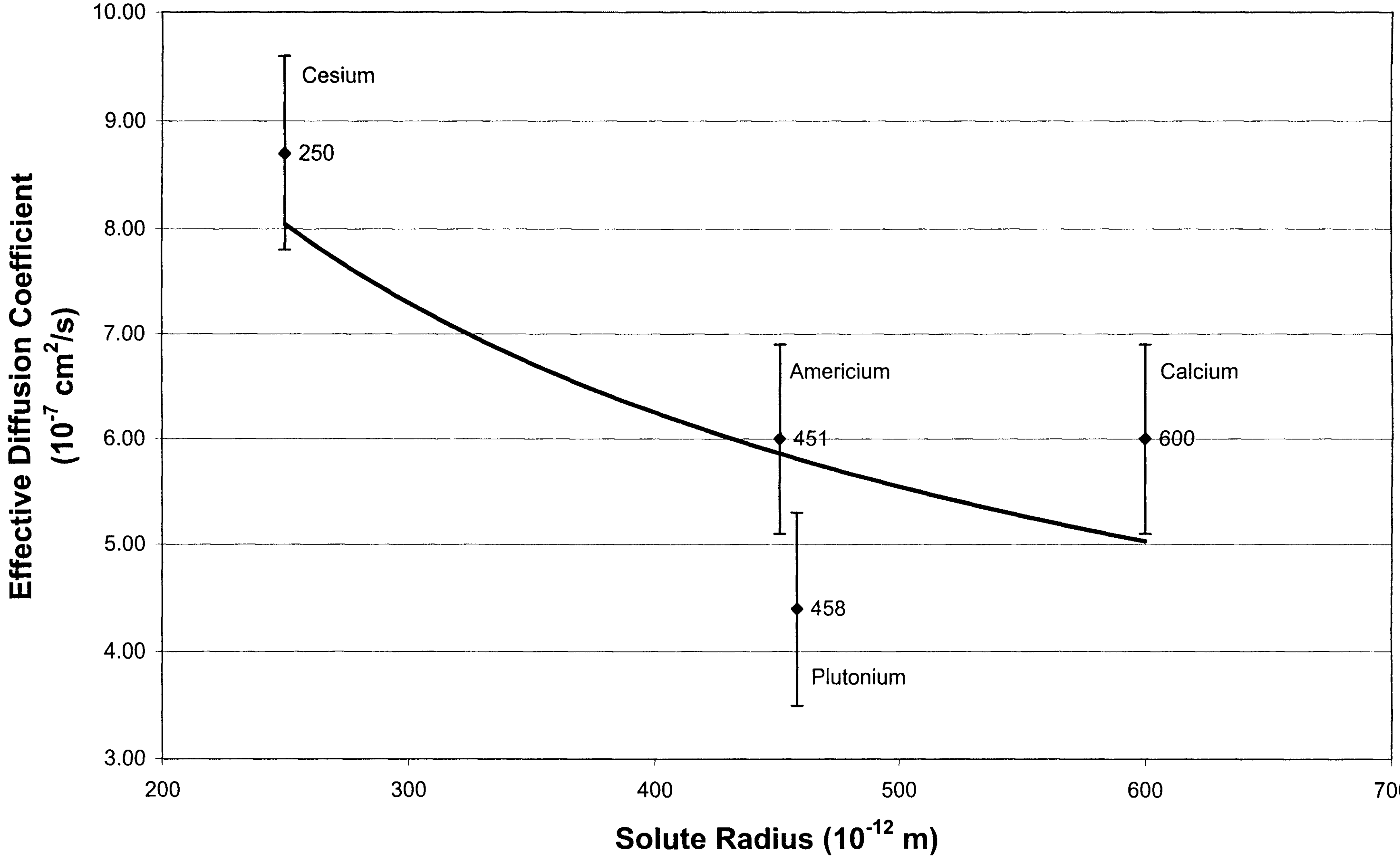

Table 3.7 – Cation Hydrated Radius Data

Cation	Hydrated Ionic Radius (10^{-12} m)	Ionic Charge
Cesium	250[a,b]	+1
Calcium	600[a,b]	+2
Americium	451[c]	+3
Plutonium	-	+4[d]
Europium	458[c]	+3

[a]Emsley 1991.
[b]Harris 1991.
[c]Fourest 1984.
[d]Plutonium determined to be present in solution as $Pu(OH)^{3+}$

3.4.5 Resistance of Transport Apparatus Bridge

Inspection of the transport experimental apparatus revealed that there were horizontal, cylindrical sections of the bridge, on either side of the membrane (Figure 3.8), that might be poorly mixed and contributing to diffusive resistance. It was still assumed to be the case that there was complete mixing (300 rpm with a 1 inch magnetic stirrer) in the feed and permeate cell sections of the apparatus. An analysis was conducted to determine if a correction in the membrane diffusion coefficient was needed to account for effective diffusion resistances in the apparatus bridge. A series of transport experiments were completed with dilute ^{14}C-labeled sucrose to estimate how the sucrose effective diffusion coefficient changed when the membrane thickness or resistance was increased, holding all other variables constant. From these data the relative resistance in the cylindrical bridge can be estimated. Equation 3.31 (Fick's Law) shows the relationship between the flux and the system resistance, where the resistance is defined as the total length of the transport distance divided by the effective diffusion coefficient (Cussler 1997, Mulder 1998).

$$J = -\frac{D_{eff}}{L_{total}}(A_f - A_r) = -\frac{(A_f - A_r)}{\left(L_{total}/D_{eff}\right)} = -\frac{(A_f - A_r)}{R_{total}} \qquad \text{Equation 3.31}$$

Where D_{eff} = System effective diffusion coefficient.
L_{Total}= Total transport length (m).
R_{Total}= Total resistance of L_{Total} (s/cm).

Equation 3.32 shows the relationship between the effective diffusion coefficient and the resistance of the apparatus bridge system in terms of the bridge mass transfer coefficient (k_B) and the membrane mass transfer coefficient (k_m). Table 3.8 provides a summary of experimentally determined effective diffusion coefficients (for L_{total}) for both

Figure 3.8 – Apparatus Bridge with Single Membrane

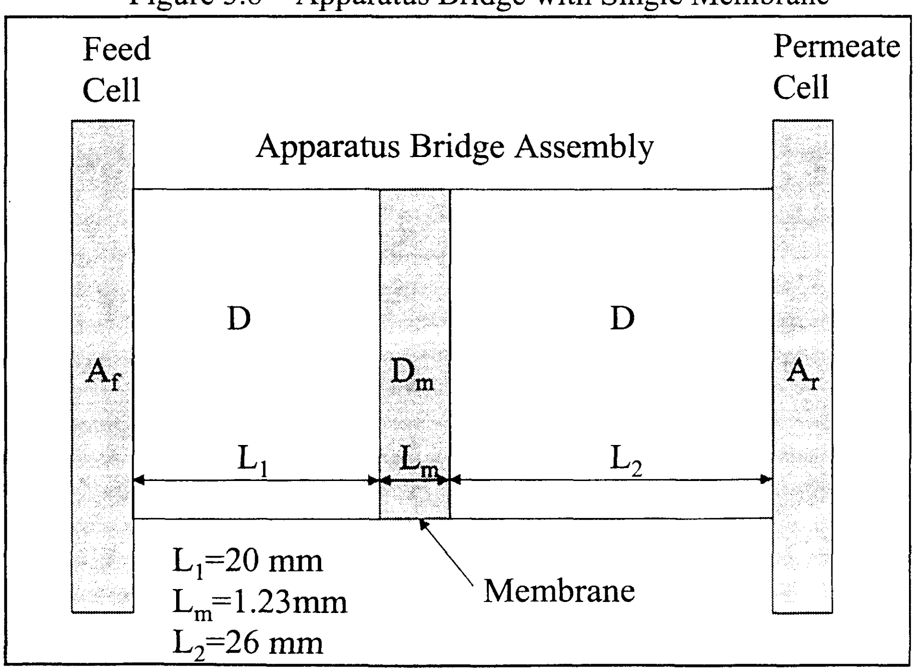

$$\frac{D_{eff}}{L_{total}} = \frac{1}{\dfrac{1}{k_B} + \dfrac{1}{k_m}} = \frac{1}{\dfrac{1}{k_B} + \dfrac{L_m}{D_m}} \qquad \text{Equation 3.32}$$

Where k_B = Bridge mass transfer coefficient.
k_m = Membrane mass transfer coefficient.
L_m= Membrane thickness.
D_m= Effective diffusion coefficient.

Table 3.8 – D_{eff} By Number of Membranes

Number of Membranes	1	2
Effective Membrane Thickness (cm)	0.123	0.246
Average Effective Diffusion Coefficient for L_{total} (10^{-5} cm^2/s)	1.3	0.67

the single and the double membrane systems neglecting resistances in the bridge assembly. Using Equation 3.32 and the D_{eff} data gathered, we determined the resistances for both the apparatus bridge ($1/k_B$) and the resistance membrane (L_m/D_m) and compared them in order to determine their relative significance. The resistances were determined to be approximately $2x10^5$ s/cm and $4x10^3$ s/cm for the membrane and bridge, respectively. This result verifies that the resistance in the bridge of the apparatus is relatively insignificant (by a factor of 50) in comparison to the resistance resulting from the membrane ($1/k_B << L_m/D_m$). With effective diffusion coefficient statistical variability greater than 24% (Section 3.4.2), we can state that the bridge resistance does not significantly contribute to the total transport resistance of the system.

3.4.6 Comparison to Alumina Membrane Study Results

Table 3.9 lists experimentally determined infinite-dilution diffusion coefficients determined for Mott® stainless steel membranes and for the alumina membranes (Bluhm 1999; Bluhm 2000). The comparison can be made in terms of order of magnitude of the effective diffusion coefficients and relative charge of the cation. Scanning electron microscopic data in referenced literature illustrates that the tortuosity of the alumina membrane honeycomb structure is approximately 1, the mean pore size was estimated to be 20 nm, the porosity 40%, and the membrane thickness 60 μm. The stainless steel membrane mean pore diameter is at least 25 times larger than that of the alumina membrane which would tend to allow a solute to more easily diffuse through the

Table 3.9 – Infinite-Dilution Diffusion Coefficients for Stainless Steel and Alumina Membranes

Cation	Initial pH	Stainless Steel D_o ($cm^2/s\ 10^6$)	Alumina D_o ($cm^2/s\ 10^6$)
Cs^+	5-7	7.0	~15
Ca^{2+}	5-7	4.5	~7.5
Eu^{3+}	2	3.7	~7.5
Am^{3+}	3.5-5	4.5	~7.5

stainless steel. However, because of the decreased porosity and increased tortuosity of the stainless steel material relative to the alumina, the cation infinite-dilution diffusion coefficients through the stainless steel membrane material were smaller than those for the alumina membranes.

When comparing cation infinite-dilution diffusion coefficients through the negatively charged alumina membrane material, the authors stated that diffusion rate of cesium (Cs^{+}) was substantially larger than that for calcium (Ca^{2+}). The authors explained the difference as evidence of the effect of charged membrane pore surfaces (i.e. electric double layer being an important effect). In summary, monovalent cations have significantly larger rates of diffusion than divalent cations as cation attraction to the pore surface was found to be proportional to cation charge. In another study by the same authors, they found that the diffusivity of iron (Fe^{+}) was substantially larger than that for americium (Am^{3+}) which was explained in a similar manner. However, because of the relative size of the estimated double layer to the size of the pore in the stainless steel membrane, there will not be a significant influence from charged pore surfaces on cation effective diffusion through the membrane.

3.4.7 Drift from Initial pH

Transport experiments were initiated at different pH in order to determine if pH influenced the transport characteristics of a particular cation. For example, calcium and cesium experiments were conducted at an initial pH of 5, 7, or 9. It was interesting to discover that with most transport experiments the pH had a tendency to drift slightly. For the purpose of determining if the membrane was the primary cause of the drift, a series of three experiments were conducted to monitor the change in pH with time. First, a transport apparatus (cell) was assembled including a stainless steel membrane, pH adjusted to 5, and the cell was placed in our ventilated hood (where all radiotracer experimentation was conducted). The second controlled experiment was identical to the first, except that the cell did not contain a membrane. The third experiment consisted of monitoring the pH of a beaker of DI water on the laboratory bench top (not in the hood) initially adjusted to pH 5. None of the three experiments contained trace amounts of radiotracer cations. Figure 3.9 shows a graphical summary of the increase in pH of all three systems with time. The exact causes of drift in the pH were not investigated. However, the most likely explanation is the slow absorption of gas from room air reacting with water to generate a basic compound, thus and increasing the pH. The general determination was made that drift occurred regardless of whether a membrane was present, the system was contained in a transport apparatus or whether the system was in the ventilation hood.

3.5 Summary and Conclusions

A series of transport experiments were conducted with five cations solutes, Cs^{+}, Ca^{2+}, Eu^{3+}, Am^{3+}, and Pu (as $Pu(OH)^{3+}$) for the purpose of determining if diffusion was the rate controlling mechanism through the Mott® stainless steel membrane material. From the transport data generated and using basic membrane characterization information detailed in Chapter 2, effective infinite-dilution diffusion coefficients were generated for each cation. These data were then compared with referenced infinite-dilution diffusion coefficients in water (no membrane) for the purpose of determining the impact of the membrane on cation transport across the stainless steel material. Results indicated that

Figure 3.9 - pH as a Function of Time

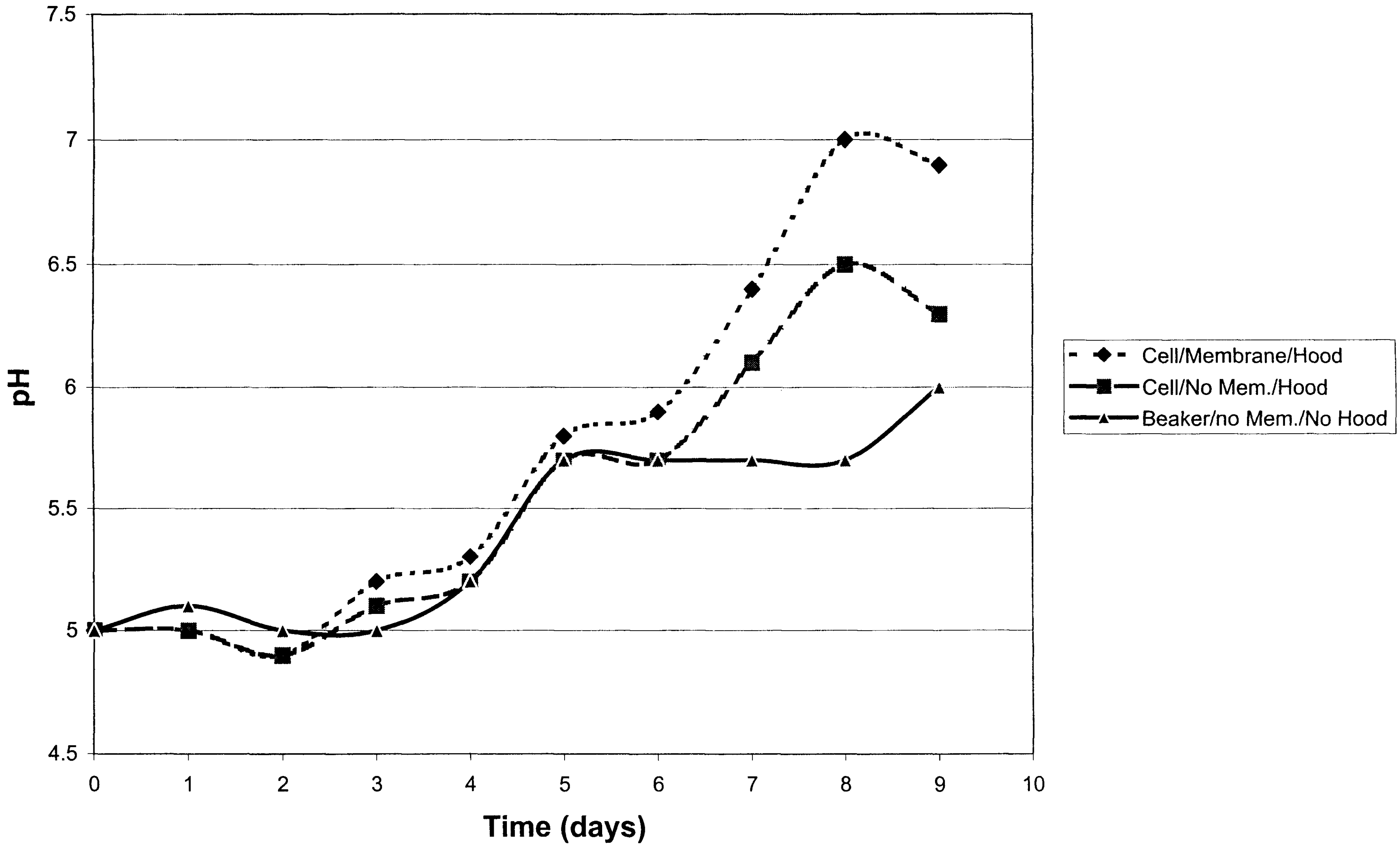

infinite-dilution diffusion coefficients from referenced literature fall within the range calculated for the experimental coefficient for Eu and Am, or were slightly higher than the experimental coefficient for Cs and Ca. Based on this information, the conclusion was made that the stainless steel membrane did not significantly influence the transport of the cations investigated under the given transport conditions indicating that diffusion is indeed the controlling mechanism which is consistent with our hypothesis.

In addition to the primary conclusion resulting from the transport data analysis, a great deal of supplemental information was gathered. Below is a summary of all the significant information and results identified concurrent with experimentation and during analysis of cation transport data.

- Effective diffusion coefficients for the given cations were easily determined by using a simple relationship between feed and permeate cell cation activities as a function of time. The relationship (Equation 3.14) was developed from Fick's Law for solute flux, system mass balances and the concentration driving force.
- No significant variance was observed in the experimentally determined effective diffusion coefficient for any of the given cations over the range of pH investigated. This information supports the hypothesis that diffusion was rate controlling for the given transport experiments, and that effects on cation diffusion rates due to electrochemical conditions of the stainless steel membrane material were not significant.

- Infinite-dilution diffusion coefficients from referenced literature were higher than the range initially calculated for the experimental infinite-dilution diffusion coefficients for the cations of interest. However, when Cs transport tests were conducted with membranes saturated with DI where trapped air had been removed (using a water miscible solution with a low surface tension prior to water saturation), the experimentally determined infinite-dilution diffusion coefficients for Cs were not statistically different than referenced values. When recalculating the remaining experimental infinite-dilution diffusion coefficients using an effective porosity which corrected for air contained in the water soaked membranes, all infinite-dilution diffusion coefficients from referenced literature were within or near the range calculated for the experimental coefficient.
- Errors caused by mass flow during the initial hours of transport (differences in cell solution volumes) were minimized by limiting the use of the early experimental data.
- Sucrose transport experimental data verified that resistances due to cylindrical sections of the apparatus bridge were small compared to the resistance due to the membrane material.
- The infinite-dilution diffusion coefficient for Pu (as $Pu(OH)^{3+}$) was not available in literature for comparison to our results. However, the

experimentally determined value of $3.3 \pm 1.3 \times 10^{-6}$ cm^2/s may have some value in the actinide industry and should be noted.

In summary, results of transport experimentation are indicate that cation diffusion is the rate controlling mechanism for the transport of the cation solutes through the stainless steel membranes tested. There were no significant variances observed in the effective diffusion coefficient for a given cations over the range of pHs investigated. Stated differently, cation diffusion was not influenced by the membrane surface (other than the effect of increased diffusion path length). Comparison of infinite-dilution effective diffusion coefficient determined experimentally and those found in literature verify that molecular diffusion through stainless steel membrane pore structures is dominant.

Chapter 4 SUMMARY

4.1 Purpose

A two part investigation was completed which determined the 1) stainless steel membrane physical characteristics and 2) transport characterization (for select solutes) of the macroporous stainless steel membrane manufactured by Mott® Metal Corporation (Farmington, Connecticut). The purpose of the investigation was to develop the basic membrane transport information in order to determine the feasibility of using porous stainless steel membranes to selectively remove actinide and non-actinide cation constituents from waste solutions, and in preparation for future investigations involving surface modification and facilitated transport studies.

4.2 Conclusions

Research verified that diffusion is the rate controlling mechanism for the transport of cation solutes through the stainless steel membranes tested. More specifically, experimental results confirmed that the Mott® stainless steel membrane surfaces do not influence transport of charged (Cs^{+}, Ca^{2+}, Eu^{3+}, Am^{3+}, and Pu^{4+}) cations, nor do the membranes influence the transport of sucrose through the material.

Physical characterization studies determined the mean pore size (diameter), pore size distribution, porosity and tortuosity of the membrane. In short, experimental results indicated that the average pore size was approximately 2.2 ± 0.5 μm, the average pore size distribution between 1.2 and 3.6 μm, the average the porosity was estimated to be 24.9 ± 5.2% using 2-isopropanol, and finally the tortuosity was estimated at 1.30 ± 0.07. Characterization results compare closely to the impenetrable sphere model and optical microscopy gray-scale analytical technique estimates.

Results of transport characterization studies showed that the experimental effective infinite-dilution diffusion coefficients compare well with those coefficients from the peer-reviewed literature. Specifically, infinite-dilution diffusion coefficients from referenced literature fall within the range (Am, and Eu) or are slightly higher than the range (Cs and Ca) calculated for the experimental infinite-dilution diffusion coefficients for the cations of interest. In addition, as a result of transport experimentation, the infinite-dilution diffusion coefficient was determined for $Pu(OH)^{3+}$ which was not found to exist prior to this work.

4.3 Recommendations

As a result of not only planned experimental preparation, experimentation and analysis, but as a consequence of experimental blunder, unexpected results (some call it serendipity, if important enough), and prodding from advisors, a number of lessons were learned during the research detailed above. Because of these lessons learned, a few recommendations should be made pertaining to equipment, experimental preparation and data analysis.

Characterization and transport experimentation has demonstrated that diffusion is the rate controlling mechanism for the transport of solutes through the stainless steel membranes tested at very dilute conditions in near neutral and acidic solutions. In addition, it was discovered that there exists significant variability in the physical characteristics of the membrane material (predominantly in the pore size distribution and void volume or porosity). These generalities assist in making the primary recommendation that this specific membrane should not be considered as a membrane to be chemically modified for facilitated transport studies. However there are several peripheral recommendations that are also worthy of note. Both the primary and less significant but important recommendations are detailed in the following paragraphs.

4.3.1 Future Investigations

Possibly the most important recommendation is that if the next phase in this research is the modification of the membrane for facilitated transport investigations, I would not recommend further use of the Mott® 316 stainless steel membrane having a nominal filtration rating of 0.5 m d u e to the variability in the membrane characteristics. Although this substrate may function well as the foundation for a more uniform membrane (asymmetric membrane) which could then be chemically modified, a narrower pore size distribution and porosity would allow much more accurate transport characterization.

4.3.2 Stainless Steel Membrane Characteriztion

Although a great deal was learned from the characterization studies described above, two principal recommendations should be provided to the reader. The recommendations deal with estimates of membrane characteristics and they are as follows:

In general, for materials with characteristics similar to the stainless steel membranes investigated in the study, the optical microscopy gray-scale analysis proved very useful tool in determining an estimate of the membrane physical characteristics. The recommendation is made to utilize this tool in the future as it provides timely, semi-quantitative estimates that can be used to direct and verify more accurate analytical techniques.

Attempts were made to determine the tortuosity from an effective diffusion coefficient which was obtained from experiments using non-radioactive sucrose and optical refractometry to measure high sucrose concentrations. This technique was difficult, at best, as concentration measurements were inaccurate. Much more accurate results were obtained when transport experiments were conducted with ^{14}C-labeled sucrose at dilute solute concentrations. However, most researchers do not have access to radiotracer counting equipment, so conducting transport experiments with non-radioactive sucrose (concentration measurements by refractometry) is a good way to estimate effective diffusion coefficient, possibly in a classroom environment.

4.3.3 Transport Experimentation

First, a substantial portion of the experimental variability involved in effective diffusion coefficients is believed to be the result of air trapped in the stainless steel membrane. Consultation with experts revealed that this fundamental mistake could have been avoided if more effort were placed on preliminary research and front work. Also, a number of experiments were conducted with americium at pH 3.5 and 5 in which there was little or no diffusion of the cation. Further investigations indicated that experimental conditions caused hydrolysis of the cation forming insoluble hydrolyzed compounds. The lesson learned, in this instance, was to thoroughly research the chemistry of constituents involved in an experimental system prior to startup in order to minimize wasted time and reduce frustration from unexpected results. Also, and maybe even more important, converse with those who have conducted similar investigations in order to acquire their insight and learn from their lessons.

Additionally, calculation of the effective diffusion coefficient from experimental transport data was initially conducted with feed or permeate cell activities (Equation 3.11 or 3.12). The resulting effective diffusion coefficients were highly inaccurate (for individual experiments) and collectively exhibited an extremely wide range due to the sensitivity of small activity changes in the permeate cell and membrane. Eventually a method of analysis was discovered that corrected for this problem: Resources suggested that since the combination of the activity in the two cells was much larger than that in the membrane and permeate cell, that the analysis should be conducted with the difference of the two relationships (Cussler 1997). Resulting effective diffusion coefficients were much more accurate and the range of coefficients narrowed. Therefore, the recommendation can be made for the use of this difference relationship (Equation 3.14) when determining transport information from similar systems.

Also, a concern was expressed as to the physical configuration of the Teflon® transport cell in that areas (the bridge) of the cell seemed prone to poor mixing and convection problems. Direct observation and analysis would indicate that the resistances in these areas were not significant, and that mixing in all portions of the cell was adequate. However, a suggestion should be made that future experiments are conducted in a modified apparatus with, as least, a shortened bridge minimizing the possibility of resistance due to poor mixing. Additionally, future researchers should consider a configuration where the feed and permeate cells are arranged vertically in order to minimize convection problems due to the physical configuration of the cell (Cussler 1997).

Another concern investigated was the influence of bulk flow on resulting transport properties. Due to the possibility of initial unequal solution volumes (creating hydraulic head) between the feed and permeate cells, data from the first 48 hours of transport experimentation was not used to calculate diffusion coefficients. Although elimination of this data did not affect the final results of this investigation, the analysis indicated that the potential for biased coefficients was high even for small volume differences (on the order of 0.1 mL) between the cells. Therefore, we recommend that the first day of transport data not be used in the determination of the diffusion coefficient unless hydraulic head differences can be eliminated.

Finally, future experiments with ionic membranes should be conducted where the pH is held constant through the use of a buffer solution. Due to pH drift at near neutral conditions, there is the distinct possibility that the relationship between cation diffusion and pH might not be as clear as it would be if the pH were continuously held constant.

REFERENCES CITED

American Society for Testing and Materials, Standard Test Method for Pore Size Characteristics of Membrane Filters Using automated Liquid Porosimeter, ASTM Standard E1294-89, 1999.

Baes, C. F., Mesmer, R. E., The Hydrolysis of Cations, Whiley-Interscience Publications, John Whiley and Sons, New York, NY, 1976.

Bird, R. B., Stewart, W. E., Lightfoot, E. N., Transport Phenomena, John Whiley and Sons, New York, NY, 1976.

Bluhm, E. A., Bauer, E., Chamberlin, R. M., Abney, K. D., Young, J. S., Jarvinen, G. D., Surface Effects on Cation Transport Across Porous Alumina Membraes, Langmuir, pg. 8668-8672, July 20, 1999.

Bluhm, E. A., Schroeder, N. C., Bauer, E., Fife, J. N., Chamberlin, R. M., Abney, K. D., Young, J. S., Jarvinen, G. D., Surface Effects on Metal Ion Transport Across Porous Alumina Membranes. 2. Trivalent Cations: Am, Tb, Eu and Fe, Langmuir, pg. 7056-7060, 2000.

Burggraaf, A. J., Cot, L., Fundementals of Inorganic Membrane Science and Technology, Elsevier, New York, NY, 1996.

Cotton, F. A., Wilkinson, G., Advanced Inorganic Chemistry, A Comprehensive Text, John Whiley and Sons, New York, NY, 1980.

Cussler, E. L., Diffusion: Mass Transfer in Fluid Systems, 2nd Edition , Cambridge University Press, Cambridge, U.K., 1997.

Cleveland, J. M., The Chemistry of Plutonium, American Nuclear Society, LaGrange Park, IL, 1979.

Emsley, J., The Elements, Second edition, Clarendon Press, New York, NY, 1991.

Fourest, B., Duplessis, J., David, D., Comparison of Diffusion Coefficients and Hydrated Radii for Some Trivalent Lanthanide and Actinide Ions in Aqueous Solution, Radiochimica Acta, Vol. 36, 191-195, 1984.

Gorden, A.J., Ford, R.A., The Chemists Companion, A Handbook of Practical Data, Techniques, and References, John Wiley and Sons, New York, NY, 1972.

Harris, D. C., Quantitative Chemical Analysis, W. H. Freeman and Company, New York, NY, 1991.

Harris, M.T., DePaoli, D.W., Ally, M., Modeling of Electrokenetic Transport of Strontium and Cesium through a Concrete Disk, Separation and Purification Technology, Vol. 11, 173-184, 1997.

Jena, A.K., Gupta, K.M., In-Plane Compression Porometry of Battery Separators, Journal of Power Sources, Vol. 80, 46-52, 1999.

Latrous, H., Ammar, M., M'Halla, J., Determination of Self-Diffusion Coefficients of 152Eu3+ Ion in Aqueous Solutions, Radiochemical Radioanalysis Letters, Vol. 55/1, 33-44, 1982.

Ma, Y. H., Mardilovich, I. P., Mardilovich, P. P., Effects of the Porosity and Pore Size Distribution of Porous Stainless Steel on the Thickness of Hydrogen Flux of Palladium Membranes, Presented at the Symposium on Membrane Technology in Petroleum, Petrochemical and Gas Processing, San Diego, CA, 2001.

Mardilovich, P. P., She, Y., Ma, Y. H., Rei, M. H. , Defect-free Paladium Membranes on Porous Stainless Steel Support, AICHE Journal, Vol. 44, 310, 1998.

Mietton-Pecchot, M., Condat, C., Courtois, T., Use of Gas-Liquid Porometry Measurements for Selection of Microfiltration Membranes, Journal of Membrane Science, Vol. 133,73-82, 1997.

Moore, D. S., McCabe, G. P., Introduction to the Practice of Statistics, W. H. Freeman and Company, New York, NY, 1989.

Mott Metal Corporation, 84 Spring Lane, Farmington Connecticut, 2000.

Mulder, M., Basic Principles of Membrane Technology, Second Edition, Kluwer Academic Publishers, Boston, MA, 1998.

Parks, G.A., The Isoelectric Points of Solid Oxides, Solid Hydroxides, and Aqueous Hydroxide Complex Systems, Chem. Rev., Vol. 65, 177-198, 1965.

Parrington, P.R.,Knox, H.D., Breneman, S.L., Baum, E.M., Feiner, F., Nuclides and Isotopes, Fifteenth Edition, General Electric Company and KAPL, Inc., San Jose, CA, 1996.

Schaep, J., vandecasteele, C., Peeters, B., Luyten, J., Dotrotremont, C., Roels, D., Characteristics and Retention Properties of a Mesoporous γ-Al2O3 Membrane for Nanofiltration, Journal of Membrane Science, Vol. 163, 299-237, 1999.

Schmid, G., Electrochemistry of Capillary Systems with Narrow Pores, I. Overview, Journal of Membrane Science, 1Vol. 50, 151-157, 1998.

Schultz, W. W., The Chemistry of Americium, ERDA Technical Information Center, Oak Ridge, TN, 1976.

Scion™ Corporation, 82 Worman's Mill Ct., Suite H, Frederick, MD, 2000.

Smith, R.M.; Martell, A.; Motekaitis, R.J. Standard Reference Database 46-Critically Selected Stability Constants of Metal Complexes, Version 3.0, 1997.

Way, J. D., Chemical Engineering and Petroleum Refining Class Notes, Membrane Separation Technologies, Colorado School of Mines, Golden, CO, 2000.

Weast, R. C., Melvin, M. J., CRC Handbook of Chemistry and Physics, CRC Press Inc., Boca Raton, Fl, 1980.

APPENDICES

Appendix I - EXPERIMENTAL PROCEDURES, EQUIPMENT SUPPLIES AND REAGENTS

I.1. Membrane Cleaning Procedure

Mott Stainless steel membranes are precut from sheet material. Disks are 25mm in diameter and approximately 0.123 to 0.124 cm thick.

1. Carefully I.D. membranes as not to damage the membrane surface.
2. Place dry membranes in the ozone generator (Borkel UVclean, model 135500). Do not stack the membranes. Set the unit to operate for 20 minutes.
3. Allow membranes to cool for 10 minutes.
4. Prepare appropriate amount (approximately 50 ml for 5 membranes) of 25% HCl.
5. Soak stainless steel membranes in the HCl for 5 minutes.
6. Prepare sonicator (Bransonic, model 2): Place 200 ml DI water in Teflon® beaker. Place membranes in Teflon® beaker. Place beaker in sonicator.
7. Fill sonicator to same water line as in Teflon® beaker.
8. Turn on sonicator and allow to run for 24 hours filling water to original level in sonicator (as needed).

9. Replace water in Teflon® beaker with fresh DI water at approximately 2 hours, 4 hours and 12 hours.
10. Check the pH of the DI water at 24 hours. If the pH is substantially lower than that of frexh DI water, continue to clean (sonicate) the membranes. Repeat this cycle until the water pH is near that of fresh DI water.
11. Remove and store membranes in dry, clean area.

Record membrane numbers, clean date and anomalies.

I.2. Transport Experimental Procedure

Tests using this procedure were conducted in a controlled environment in Technical Area 48 at the Los Alamos National Laboratory. Facility and laboratory specific training was required in order to conduct experimentation with the radiotracers (^{14}C impregnated sucrose, ^{137}Cs, ^{45}Ca, ^{152}Eu, ^{241}Am, and ^{239}Pu), in case of emergency conditions and for waste disposal.

1. Prepare 1M, 0.01M, and 1×10^{-4} M (slightly acidic or basic) HNO_3 and NaOH solutions for pH adjustment. Prepare 0.1M $NaNO_3$ for ion concentration adjustment.

Record solution information.

2. Obtain radiotracer cation stock solution.

Record cation solution information (activity, acidity, etc.).

3. Obtain a cleaned stainless steel membrane (Appendix I.1).

   Record membrane I.D.

4. Obtain and assemble multiple position stir plate. Place stir plate in adequate safety containment for system operation.
5. Obtain pH meter (Orion, model 900A) and stock of buffer solutions.
6. Obtain appropriate scintillation sample vials (50ml) with 10ml scintillation cocktail for alpha/beta counter (Ca, Eu, Am and Pu) or 10ml water for gamma counter (Cs).
7. Obtain a complete transport cell which is comprised or 2 Teflon-200ml cell halves, 6 piece Teflon bridge (2-O-rings, bridge wedge, 2-threaded cell ports, and clamp), 2-Teflon caps, and two magnetic stir rods.

   Record cell number and condition.

8. Clean and assemble the transport cell, including membrane.
9. Check the transport cell for leaks by filling both sides of the cell with amount of D.I. water and 0.1M $NaNO_3$ required for given test. Allow the cell to stand for one day and periodically check for leaks. If leaks are observed, drain the cell, replace part(s), if necessary, reassemble the cell and again check for leaks.

   Record amounts of DI water and $NaNO_3$.

10. Calculate NaOH or HNO_3 needed to adjust pH based on D.I. water pH and cation stock specifications.

    Record calculations.

    Note: Tests are based on 100ml solution in both feed and permeate side of transport cell, and 1.0E-3M $NaNO_3$.

11. Place the cell on the stir plate (300 rpm) making sure that feed and permeate sides of cell are well labeled.
12. Calibrate pH meter for desired pH range.
13. Adjust permeate cell to pH called for in test matrix using HNO_3 and NaOH solutions.

    Record permeate cell initial pH.

14. Verify that pH of feed cell is below 3.0 for americium and plutonium experiments (cations hydrolyze and precipitate above this pH). This is not a concern for other ions being tested.
15. Add calculated amount of radiotracer stock solution to the feed cell.

    Record radiotracer stock solution information and volume added.

16. After mixing for 5 minutes, sample feed and permeate cells.
17. Adjust feed cell to pH called for in test matrix matrix using HNO_3 and NAOH solutions.

    Record feed cell initial pH.

18. Sample feed and permeate cells once daily.

    Record feed and permeate cell sample I.D. and times sampled.

19. Experiment duration should be approximately two weeks.
20. When experiment is complete, measure final pH for both feed and permeate.

    Record feed and permeate final pH.

21. Dispose of cell solutions as appropriate.
22. Disassemble cell and place membrane in scintillation sample vial for counting.

    Record membrane appearance and sample vial information.

23. Clean disassembled transport cell with industrial soap and water for future use.
24. Count samples with the Packard NaI Gamma Counter model 5000 (^{137}Cs) or the Wallac Liquid Scintillation Counter model 1414 (^{14}C impregnated sucrose, ^{45}Ca, ^{241}Am, ^{152}Eu, and ^{239}Pu).

I.3 Pore Size Distribution Procedure (Flow Porometer)

Tests using this procedure were conducted at the Colorado School of Mines. A flow porometer was assembled (see equipment list) and compressed nitrogen used as the test gas. Membranes were held in a Millipore membrane cell that had been modified for the 0.123 to 0.124 cm thick Mott stainless steel membranes

1. Obtain a clean (Appendix A-1.1) Mott® stainless steel membrane.

   Record membrane information (number).

2. Completely wet the inner void volume of the membrane by soaking it in the wetting solution for given time period. Note soak time if other than 3 days.

   Record wetting solution type and soak time information.

2. Verify that there is gas in the nitrogen supply tank by opening the tank supply valve and noting the tank pressure.
3. Remove the Millipore® membrane cell from the porometer apparatus.
4. Clean the thread tape from the inlet and outlets of the cell and apply new Teflon® tape.
5. Place the wetted membrane in the Millipore® cell. Firmly torque the set-screws on the cell, taking care not to over torque.
6. Reassemble the porometer being careful not to over torque the cell inlet and outlet fitting nuts.
7. Slowly increase the inlet pressure on the cell by manipulating the feed gas needle valve. Hesitate when the flow meter ball just begins to lift from the bottom of the meter.

   Record inlet pressure at indication of initial flow.

8. Incrementally increase the feed side pressure and record corresponding flow meter reading. This procedure should be conducted as quickly as possible while maintaining accuracy as to minimize wetting solution evaporation.

    Record wet membrane test inlet pressure and flow meter reading.

9. Discontinue wet membrane test when maximum flow rate (maximum reading on flow meter) has been achieved.
10. Dry the membrane at maximum nitrogen flow rate for a period of time sufficient for wetting solution evaporation. Experiments with DI water are to be dried for 3 hours and those with 2-Isopropanol for 30 minutes.

    Record drying time period.

11. Incrementally increase the feed side pressure and record corresponding flow meter reading. This procedure should be conducted as quickly as possible while maintaining accuracy as to minimize wetting solution evaporation.

    Record dry membrane test inlet pressure and flow meter reading.

12. Remove the cell from the porometer apparatus in preparation for additional tests.
13. Calculate pore size distribution using spreadsheet.

I.4 Porosity Experimental Procedure

Tests using this procedure were conducted at the Colorado School of Mines. The procedure was design to measure the void volume of the Mott® stainless steel membrane with a low surface tension liquid (2-isopropanol) as no special provisions were made to remove air from membrane material void volumes.

1. Obtain a clean (Appendix I.1) Mott® stainless steel membrane.

   Record membrane information (number).

2. Dry the membrane for 1 hour by flowing nitrogen at maximum flow meter rate (a rate of approximately 15 L/minute) using the pore size distribution apparatus or porometer.
3. Weigh the dried Mott® stainless steel membrane.

   Record membrane weight.

4. Submerge and soak membrane in designated solvent for given time period.

   Record solvent and time.

5. Remove membrane from solvent. Quickly, remove visible liquid from the surface of the membrane and weigh.

   Record wet weight.

6. Repeat soak and weigh as necessary (repeatability experiemnts).
7. Calculate Porosity.

I.5 Equipment and Reagents

Basic Equipment:

1. Borkel® UVclean Ozone generator/Cleaner, model 135500
2. Bransonic® Ultrasonic Cleaner, model 2
3. Packard® NaI Gamma Counter model 5000
4. Wallac® Liquid Scintillation Counter model 1414
5. Variomag® Multiple Position Stir Plate
6. Transport Cell
   2 Teflon® -200ml cell halves,
   6 piece Teflon® bridge (2-O-rings, wedge, 2-threaded cell ports, and clamp),
   2-Teflon® caps,
   2 magnetic stir rods
7. Orion® pH meter, model 900A
8. Eppendorf® Pipet (0.025-1.000ml)
9. Sample Vial Stand
10. Porometer
    2 Gauges, 0-100 psig
    Millipore® High Pressure SST Filter Holder
    Cole-Parmer Flowmeter, 316 SS, 0-16 L/hr
    Swagelock Fittings and Tubing
11. Mettler® AT20 Balance

Supplies

1. Mott® Stainless Steel Membrane Sheet
2. Scintillation Sample Vials (50ml)
3. Pipet Tips
4. Chemical Resistant Gloves
5. Masking Tape
6. Safety Glasses
7. 50ml, 100ml, 500ml Glass Beakers
8. 250ml Teflon® Beakers
9. Miscellaneous Plastic Bags
10. Cardboard Waste Containers
11. 5-Gallon Liquid Waste Containers
12. Vermiculite®
13. Compressed Nitrogen
14. Teflon® Pipe Tape

Commercially available, reagent-grade chemicals were obtained for use during experimentation. Listed below are the general chemicals used.

Reagents/Chemicals:

	Reagent	Specifications
1.	De-ionized (DI) Water	In House
2.	HNO_3	Liquid (15.8M) - Reagent Grade
3.	NaOH	Liquid (50%) - Reagent Grade
4.	$NaNO_3$	Solid - Reagent Grade
5.	Ultima Gold Scintillation Cocktail	Packard Specifications
6.	2-Isopropanol	500 ml

Appendix II - Detailed Pore Size Distribution Data

Table A.1 – Pore Size Distribution Data

Membrane	Solvent	Mean Pore Diameter - D_p (μm)	Distribution (μm)
1(old)	DI	4.5	2.5-9.8
2(old)	DI	4.5	3.2-8.4
4(old)	DI	4.8	3.2-9.0
5(old)	IP	4.2	2.26.3
6(old)	IP	4.1	2.3-6.3
N1	IP	1.3	0.8-2.1
N19	IP	2.2	1.2-4.2
N2	IP	1.3	0.7-2.1
N20	IP	2.6	1.4-4.2
N24	IP	2.3	0.9-4.2
N25	IP	1.8	1.3-4.2
N3	IP	1.1	0.7-2.1
N4	IP	1.3	0.9-2.1
N5	IP	1.3	0.7-2.1
N6	IP	1.2	0.7-2.0
N7	IP	1.2	0.6-2.4
N8	IP	1.4	0.6-4.3
O1	IP	2.7	1.4-4.2
O2	IP	2.5	1.8-4.2
O3	IP	2.8	1.4-4.2
O4	IP	2.6	1.8-4.2
O5	IP	2.9	1.6-4.2
O6	IP	2.9	1.4-4.2
Average (IP) =		2.2 ± 0.5	1.2-3.6

Note: Membrane disks were machined from two stock sheets of material. Sheet one (1) designated by "old", "O" or no designation, and sheet two (2) designated as "N".

Appendix III. Detailed Porosity Data

Table A.2 – Porosity Data

Membrane	Solvent	Dry (g)	Wet(g)	Soak t (day)	Void (%)
1	DI	3.5411	3.6261	3	15.8
2	DI	3.5208	3.6319	3	19.8
3	DI	3.5569	3.6557	0.25	17.8
4	DI	3.5193	3.6081	0.25	16.4
5	DI	3.5475	3.6318	0.25	15.6
7	IP	3.4402	3.6333	3	35.8
8	IP	3.5312	3.6586	3	26.4
9	IP	3.5654	3.6795	3	24.1
N1	IP	3.5587	3.6510	3	20.5
N2	IP	3.5703	3.6878	3	24.6
N3	IP	3.5637	3.6802	3	24.5
N4	IP	3.5736	3.6914	3	24.7
N5	IP	3.5463	3.6619	3	24.5
N6	IP	3.5607	3.6758	3	24.3
N7	IP	3.5657	3.6816	3	24.4
N8	IP	3.5667	3.6608	3	20.8
O1	IP	3.5442	3.6590	3	24.3
O2	IP	3.5537	3.6718	3	24.8
O3	IP	3.5225	3.6379	3	24.5
O4	IP	3.5173	3.6361	3	25.1
O5	IP	3.5069	3.6226	3	24.7
O6	IP	3.5440	3.6983	3	30.2
N13	IP	3.5505	3.6663	3	24.5
N14	IP	3.5741	3.6928	3	24.8
N15	IP	3.5604	3.6769	3	24.5
N16	IP	3.5563	3.6654	3	23.4
N17	IP	3.5514	3.6737	3	25.5
N18	IP	3.5656	3.6853	3	25.0
N19	IP	3.5641	3.6824	3	24.8
N20	IP	3.5431	3.6588	3	24.5
N21	IP	3.5527	3.6664	3	24.1
N22	IP	3.5587	3.6770	3	24.8
N23	IP	3.5671	3.6706	3	22.4
N24	IP	3.5554	3.6741	3	24.9
N25	IP	3.5362	3.6563	3	25.2
N26	IP	3.5668	3.6870	3	25.1
Average De-ionized Water (DI)					17.1± 4.8
Average 2-Isopropanol (IP)					24.9 ± 5.2

Note: Membrane disks were machined from two stock sheets of material. Sheet one (1) designated by "old", "O" or no designation, and sheet two (2) designated as "N".

Table A.3 – Porosity Error Calculation Data

Membrane I.D. (%)	ε at 5 Days (%)	ε at 5 Days (%)	ε at 5 Days (%)	Average ε for given Membrane (%)
N17	25.5	25.6	25.8	25.6 ± 0.1
N18	27.2	27.7	27.6	27.5 ± 0.2
N19	26.8	27.3	27.5	27.2 ± 0.4
N20	23.1	22.9	23.2	23.1 ± 0.0
N21	24.3	24.1	24.5	24.3 ± 0.1
N22	26.0	26.1	25.6	25.9 ± 0.2
N23	25.0	25.5	25.2	25.3 ± 0.2
N24	25.5	25.7	26.0	25.7 ± 0.2
N25	22.7	22.5	22.9	22.7 ± 0.2
N26	27.5	27.1	27.2	27.3 ± 0.1
Average ε for given Membrane (%)				25.5 ± 0.2

Appendix IV - Detailed Transport Experimental Data

Table A.4.1 – Calcium Transport Experimental Activity Data

Run	Net Permeate Activity (cpm)	Net Feed Activity (cpm)	Cummlative Time (hours)	Run	Net Permeate Activity (cpm)	Net Feed Activity (cpm)	Cummlative Time (hours)
Ca4B	0	471.7	0	Ca1C	0	736.5	0
	1.4	410.9	1.25		11.4	773.4	23.17
	6	378.5	48.42		16.6	757.6	47.17
	13.3	382.2	71.83		24.7	719.5	75.1
	21.4	393.6	95.83		42.3	744.3	102.38
	47.9	392.2	168		48.1	732.4	144.73
	56.1	379.9	220.15		77.2	713.3	216.38
	71.6	358.3	260		93.3	751.4	263.97
					181.5	695.7	383.63
Ca4D	10.6	793	23.17	Ca4H	0	452.3	19.17
	18.1	595.9	102.38		10.6	449.3	42
	21.4	654.7	125.38		8.3	433.1	64.6
	41.8	618	216.38		12.3	459.1	89.5
	47.6	603.6	263.97		23.8	450.2	185.75
	62.9	582.9	338.38		24.2	455.8	209.63
	85	626.6	383.63		25.5	455.4	234
					33.7	466	339.48
					39.3	450.6	360.06
Ca5B	-3.4	387.7	1.25	Ca5E	0	408	0
	1.4	371	24.6		9.4	345.8	20
	7.6	397.9	48.42		16.1	339.9	70.84
	16.6	374.3	71.83		18.2	326.6	92.92
	21.8	374.6	95.83		20.9	321.9	117.34
	38.1	396.1	168		21.1	257.6	140.67
	45.1	374.7	220.15		21.1	116.2	238.75
	68.5	370.5	260		63.3	352.8	244.92
					66.3	329.9	284.92

Table A.4.1 – Calcium Transport Experimental Activity Data (cont.)

Run	Net Permeate Activity (cpm)	Net Feed Activity (cpm)	Cummlative Time (hours)	Run	Net Permeate Activity (cpm)	Net Feed Activity (cpm)	Cummlative Time (hours)
Ca6G	4.2	669.6	0	Ca3A	15.7	1970.5	1
	11	568.7	15.47		8.5	1970.4	2
	8.5	580.5	38.89		14.2	1912.5	6.25
	16.7	597	62.94		15.7	1934.9	7
	17.5	589.9	86.56		43.7	1849.5	27.08
	27.1	592.7	109.81		216.05	1863.65	145.5
	32.9	569	135.81		236.05	1778.75	170.42
	41.7	586.1	159.27		465.1	2021.8	246
	37.1	556.2	182.67		333.7	2104.1	268.67
	41.9	559.3	257.72		518.8	2121.1	295.67
	49.1	550.8	278.47		494.5	1847.2	319.17
	55.4	571.1	288.42		563.3	1574.6	410.8
					580.6	1619.2	432.67
					609.7	1611.7	457.41
					612.6	1970.4	481.83
					819.2	1598.3	602.5
Ca3F	-6.9	634.1	0	Ca6B	7.7	468.1	0
	20	671.5	17.67		0.6	417.2	1.25
	26.4	664	40.83		4.7	406	24.6
	45.6	624	111.03		12.4	414.6	48.42
	55.6	648.1	135.43		44.1	418.6	71.83
	68.4	619.7	159.18		31.6	412.4	95.83
	75.1	620.1	236.1		46.1	418.4	168
	100.8	606.6	255.02		73.9	409.5	220.15
	110.4	646.6	282.19		99.4	392.9	260
Ca7G	0	477.2	0				
	5.2	445.6	15.47				
	5.8	435.2	38.89				
	14.6	447.7	62.94				
	13.7	447	86.56				
	13.7	525.6	109.81				
	20.8	425.8	135.81				
	22.9	589.3	159.27				
	27.3	448.9	182.67				
	40.5	430.6	257.72				
	47.6	438.8	278.47				
	46	427	288.42				

Table A.4.2 – Cesium Transport Experimental Activity Data

Run	Net Permeate Activity (cpm)	Net Feed Activity (cpm)	Cummlative Time (hours)	Run	Net Permeate Activity (cpm)	Net Feed Activity (cpm)	Cummlative Time (hours)
Cs5A	0	477.2	0	Cs1B	2	7518	0
	5.2	445.6	15.47		188	7428	18.17
	5.8	435.2	38.89		1526	6155	186.5
	14.6	447.7	62.94		1672	5972	216.67
	13.7	447	86.56		1702	5842	234.5
	13.7	525.6	109.81		2192	4926	353.25
	20.8	425.8	135.81		2580	4544	476
	22.9	589.3	159.27		2690	4601	496.67
	27.3	448.9	182.67		2733	3767	595.17
	40.5	430.6	257.72				
	47.6	438.8	278.47				
	46	427	288.42				
Cs1C	-8	5902	0	Cs9E	8	8041	0
	67	5315	23		67	7920	24.58
	188	4877	53.08		101	7860	47.92
	252	5629	71.08		157	7854	72.15
	345	6044	94.33		212	7752	95.42
	640	5744	171.9		278	7813	121.42
	849	5502	237.15		341	7636	144.87
	1335	5097	391.08		619	7566	264.17
	1363	5124	407.08		660	7417	288.42
Cs2B	-2	7437	0	Cs2C	-8	5902	0
	48	7299	18.17		67	5315	23
	666	6647	186.5		188	4877	53.08
	772	6631	216.67		252	5629	71.08
	830	6303	234.5		345	6044	94.33
	1158	5850	353.25		640	5744	171.9
	1326	5600	476		849	5502	237.15
	1548	5547	496.67		1335	5097	391.08
	1663	4763	595.17		1363	5124	407.08
Cs2D	-3	7174	0	Cs6F	8	7736	0
	174	7087	17.67		98	7714	19.17
	413	6897	40.83		167	7631	42
	836	6363	88.17		288	7522	64.6
	1025	6220	111.03		352	7415	89.5
	1251	6080	135.43		620	7160	163
	1400	5962	159.18		691	7082	185.75
	1881	5433	236.1		780	7008	209.63
	2004	5451	255.02		876	6909	234
	2103	5167	282.19		970	6926	256.75
					1249	6650	339.48
					1341	6579	360.06

Table A.4.2 – Cesium Transport Experimental Activity Data (cont.)

Run	Net Permeate Activity (cpm)	Net Feed Activity (cpm)	Cummlative Time (hours)	Run	Net Permeate Activity (cpm)	Net Feed Activity (cpm)	Cummlative Time (hours)
Cs6G	76	19569	0	Cs1G	23	18667	0
	150	18901	19		370	18395	19
	392	18346	43		732	18260	43
	665	17992	66		1075	18920	66
	873	18001	91.17		1471	17983	91.17
	1270	17829	123.75		1965	17476	123.75
	1480	17504	144.5		2303	17604	144.5
	1682	16935	162.08		2489	17193	162.08
	2157	16888	213		3270	16456	213
	2618	16325	260		3593	15589	260
Cs2G	24	18589	0	Cs3G	25	19682	0
	70	18645	19		161	19795	19
	175	18733	43		284	19924	43
	295	19535	66		477	20095	66
	454	18949	91.17		717	20280	91.17
	624	18839	123.75		986	20486	123.75
	735	18537	144.5		1197	20347	144.5
	885	19121	162.08		1382	20070	162.08
	1129	18282	213		1895	19890	213
	1349	17776	260		2389	20191	260
Cs5G	51	18863	0	Cs9G	10	18819	0
	370	18866	19		215	19795	19
	667	18878	43		440	20558	43
	1047	18613	66		856	19801	66
	1389	17442	91.17		1280	19779	91.17
	1869	17828	123.75		1952	19243	123.75
	1533	16324	144.5		2169	19013	144.5
	2360	17825	162.08		2501	18578	162.08
	2986	16170	213		3204	17885	213
	3555	15255	260		3781	17032	260
Cs7F	11	7581	0				
	90	7617	19.17				
	156	7621	42				
	208	7508	64.6				
	271	7394	89.5				
	442	7324	163				
	508	7390	185.75				
	547	7316	209.63				
	602	7095	234				
	671	7112	256.75				
	815	7052	339.48				
	855	7091	360.06				

Table A.4.2 – Cesium Transport Experimental Activity Data (cont.)

Run	Net Permeate Activity (cpm)	Net Feed Activity (cpm)	Cummlative Time (hours)	Run	Net Permeate Activity (cpm)	Net Feed Activity (cpm)	Cummlative Time (hours)
Cs4A	138	108019	0	Cs3B	106	6824	0
	809	102360	1.25		144	6695	18.17
	3615	115594	16.66		1371	5855	186.5
	4080	115463	19.5		1531	5816	216.67
	5024	114971	24.91		1571	5366	234.5
	7388	106043	41.83		2047	4651	353.25
	15377	85279	116.55		2384	4477	476
	17756	82091	138.56		2541	4372	496.67
	20425	81036	163.21		2566	3691	595.17
	22637	78895	187.55				
	36548	80111	308.33				
	37378	76578	336				
	39125	75766	357.92				
	41382	72687	381.84				
	43552	72789	425.84				
	40103	61196	476.12				
	41787	59387	523.34				
	42333	58379	570.71				
	45647	65290	666.89				
	46093	54803	714.94				
	47188	53371	811.76				
	48108	52975	859.12				
Cs7G	80	19498	0	Cs3C	8	5610	0
	105	19430	19		84	4824	23
	288	18511	43		172	5148	53.08
	438	18428	66		231	5848	71.08
	601	18428	91.17		279	5725	94.33
	828	18554	123.75		461	5588	171.9
	977	18425	144.5		631	4528	237.15
	1108	18225	162.08		924	5258	391.08
	1452	17906	213		943	5194	407.08
	1686	17351	260				

Table A.4.3 – Europium Transport Experimental Activity Data

Run	Net Permeate Activity (cpm)	Net Feed Activity (cpm)	Cummlative Time (hours)	Run	Net Permeate Activity (cpm)	Net Feed Activity (cpm)	Cummlative Time (hours)
Eu4A	77.9	7666.6	0	Eu4B	-25.4	7514	0
	326.9	7902.3	23.75		150.1	7108.7	18.83
	459.4	7851	47.08		198.6	7083.7	42.83
	573.5	7995.9	73.25		281	7089.3	66.5
	658.2	7842.1	95.08		340.4	7089.4	91.5
	970.6	9960	95.08		631.4	6217.6	235.67
	1053.3	7992.7	193		683.3	6172	258.08
	1180.8	8005.5	216				
	1227.3	7971.1	240				
	1504.9	8220.7	287.66				
	1647.8	7963.2	333.99				
	1754.9	7580.1	359.74				
	1929.9	7779.9	406.99				
	2323.6	7812.3	501.74				
	2696.7	7507.1	550.74				
Eu1C	34.7	4449.9	0				
	343.4	4530.7	19.91				
	436.3	4560.4	69.85				
	462.8	4600.9	96.83				
	508.8	4432.2	123.03				
	546.2	4041.3	140.36				
	589.7	3816.5	167.28				
	629.6	3801.9	248.7				
	704.9	4044.1	282.95				
	773.7	3791.9	306.94				

Table A.4.4 – Americium Transport Experimental Activity Data

Run	Net Permeate Activity (cpm)	Net Feed Activity (cpm)	Cummlative Time (hours)	Run	Net Permeate Activity (cpm)	Net Feed Activity (cpm)	Cummlative Time (hours)
Am1A	21.4	1690.2	0	Am2A	-3	1750.1	0
	17.9	2481	1.33		5.3	1773.5	1.33
	25.9	2848.4	2.92		9.9	2647.4	2.92
	33.1	2842.2	4		13.1	2773.7	4
	27	2895.4	6.83		9.5	2829.1	6.83
	51.8	2797.8	23.67		46.8	2804.7	23.67
	40.6	2801.1	26.67		11.2	2667.2	26.67
	53.7	2804.46	47.33		11.9	2762.7	47.33
	448.8	2749.5	71.33		18.3	2744.1	71.33
	89.6	2415.2	97.17		18.3	2340.6	97.17
	104.8	2382	121.33		27.3	2430.7	121.33
	132.7	2391.9	145.9		33.3	2392.8	145.9
	148.3	2345.3	168.58		40.2	2385.1	168.58
	175.8	2386.2	190.88		46.5	2410.9	190.88
	245.5	2277.8	265.17		73.1	2369	265.17
	293.6	2235.6	289.17		78.9	2389.5	289.17
	306.5	2242.2	312.17		90.6	2359.1	312.17
	333.3	2169.2	336.17		93.5	2382.2	336.17
	361.3	2150.9	360.17		109.1	2322.5	360.17
	444.7	2092	457		142.3	2227	457
	471.5	2016.7	481.48		147.7	2274.7	481.48
	403.9	1716	504.33		141.7	1586.6	504.33
	570.3	1974.1	529		167.7	2237.9	529
	588.9	1990.2	549.92		182.9	2041.3	549.92
	625.1	1936.8	598.67		224.5	2225.4	598.67
	671.7	1903.1	694		238.6	2146.4	694
	737	1814.8	767.67		277.3	2112.9	767.67
	771.7	1764.2	815.58		269.2	2026.2	815.58
	775.3	1693.9	838.33		273.9	1991.3	838.33
Am9E	3.1	900.5	0	Am1F	2	419.2	0
	42.9	840.4	23.33		4.5	484.3	37.92
	51	877	46.75		7.6	474.2	60.52
	63.9	865.5	70.08		14.8	462	85.42
	80.4	856.9	94.42		28.3	476.2	158.92
	70.4	843.8	117.67		34.6	477.6	181.67
	76.3	844.3	143.67		32.9	451.9	205.55
	94.5	838.5	167.13		46.9	426.3	229.92
	103.2	835.5	190.53		47.1	446.6	252.67
	123.3	798.3	265.58		64.5	433.9	335.4
	137.5	792.1	286.33		69.3	414.2	355.98
	150.3	764.3	310.58				

Table A.4.4 – Americium Transport Experimental Activity Data (cont.)

Run	Net Permeate Activity (cpm)	Net Feed Activity (cpm)	Cummlative Time (hours)	Run	Net Permeate Activity (cpm)	Net Feed Activity (cpm)	Cummlative Time (hours)
Am9D	-0.6	633	0	Am1E	0	843.5	0
	3.1	623.3	15.58		4.8	859.1	23.33
	29.8	674.1	66.42		3.9	853.9	46.75
	37.1	552.9	88.5		6.3	857.5	70.08
	32.5	550.7	112.9		6.7	844.8	143.67
	30.8	383.2	136.25		12.4	829.4	167.13
	56.1	304.9	234.33		10.7	845.3	190.53
	106.8	747.1	240.5		17	872.6	265.58
	121.8	708.9	280.5		20.5	869.6	286.33
Am2E	0.2	954.9	0				
	2.4	635.1	23.33				
	10.6	650.8	46.75				
	11.4	651.3	70.08				
	28.9	667.8	143.67				
	28.7	661.9	167.13				
	35.5	715.8	190.53				
	53.6	641.3	265.58				
	55.6	681.9	286.33				

Table A.4.5 – Plutonium Transport Experimental Activity Data

Run	Net Permeate Activity (cpm)	Net Feed Activity (cpm)	Cummlative Time (hours)	Run	Net Permeate Activity (cpm)	Net Feed Activity (cpm)	Cummlative Time (hours)
Pu1A	17.9	2481	1.33	Pu4B	0.1	6862	0
	25.9	2848.4	2.92		209.9	6952.8	19.91
	33.1	2842.2	4		393	6930.9	69.85
	27	2895.4	6.83		446.6	6730.6	96.83
	51.8	2797.8	23.67		519.3	6773.1	123.03
	40.6	2801.1	26.67		495.2	6692.2	140.36
	53.7	2804.46	47.33		676.7	6583.7	167.28
	89.6	2415.2	97.17		761.2	5714.8	248.7
	104.8	2382	121.33		895.5	6037	282.95
	132.7	2391.9	145.9		944.8	5889	306.94
	148.3	2345.3	168.58				
	175.8	2386.2	190.88				
	245.5	2277.8	265.17				
	293.6	2235.6	289.17				
Pu1C	150.8	8624.2	0	Pu1D	3.6	9180.1	0
	75.4	4146.3	21.58		135.9	9075	24.3
	144.3	4141.6	72.42		210.4	9274.4	41.58
	183.2	3777.2	94.5		291.7	8932.1	67.23
	219	4093.5	118.92		421.3	8411.3	99.33
	242.5	3830.9	142.25		472.8	8607.3	118.27
	147.3	1663.5	240.33		564.4	8622.6	143.67
	459	4421.2	246.5		613.8	8382.7	165.18
	532.5	4369.2	286.5		965.9	8296.9	232.83
Pu5B	-2.7	6708.1	0	Pu2C	49.8	10647	0
	129.7	6942.2	19.91		14.3	5037.8	21.58
	246.2	6885.1	69.85		57	5138.1	72.42
	303.5	6821.6	96.83		66.3	5287.2	94.5
	388.5	6768.9	123.03		94.9	5097.1	118.92
	480.1	6628.1	167.28		108.1	4548.1	142.25
	623.7	5920.9	248.7		85.6	2127.8	240.33
	716.3	6228.7	282.95		258.6	5621.7	246.5
	762.9	5773.8	306.94		320.8	5238.4	286.5
Pu2D	5.4	9229.3	0	Pu3D	1.3	9449.8	0
	105.7	8577.9	24.3		235.1	9113.6	24.3
	176.5	8697	41.58		305	9031.8	41.58
	272.3	8618	67.23		403	8963.5	67.23
	378	8485.7	99.33		510	8737.9	99.33
	458.7	8621.7	118.27		581.5	8676.2	118.27
	522	8288.4	143.67		697.4	8686.6	143.67
	620.9	8297.7	165.18		794.2	8591.9	165.18
	890.7	8122.3	232.83		1075	8485.5	232.83

Table A.4.5 – Plutonium Transport Experimental Activity Data (cont.)

Run	Net Permeate Activity (cpm)	Net Feed Activity (cpm)	Cummlative Time (hours)	Run	Net Permeate Activity (cpm)	Net Feed Activity (cpm)	Cummlative Time (hours)
Pu3A	1.8	8576.3	0	Pu6B	0.3	5924.3	0
	61	8547.3	48		90	4858	19.91
	36.1	8618.2	65.22		189.6	5406.6	69.85
	66.2	8700.8	91.05		241.7	5289.6	96.83
	75.3	8657.8	114.72		282.6	5293	123.03
	83.2	8760.9	138.05		254.5	4530.4	140.36
	102.4	8779.5	234.8		321.9	4828.2	167.28
	128.9	8643.4	261.38		460	4734.7	248.7
	125.5	8638	287.6		499.7	4598.2	282.95
	175.5	8732.6	336.22		545	4466.7	306.94
	172.2	8721.4	360.22				
	177.3	8759	384.22				
	188.9	8405.8	424.8				
	213	8349	454.75				
Pu3C	16.7	5592.2	0	Pu9E	19.6	8758.4	0
	63.8	3415.5	21.58		171.9	8407.7	19.17
	123.2	3202.2	72.42		216.3	8028.3	42
	151.2	2772.6	94.5		272	7751.5	64.6
	195.1	3070.5	118.92		337.6	7626.8	89.5
	197.6	2743.7	142.25		608.1	6941.8	163
	136.7	1517.7	240.33		670.8	6555.2	185.75
	392.2	3427.2	246.5		765.3	6241	209.63
	431.8	3405.6	286.5		814.7	5837	234
					897.2	5340.2	256.75
					1067.4	4881.2	339.48
					1129.5	4747.9	360.06

Table A.4.5 – Sucrose (^{14}C) Transport Experimental Activity Data

Run	Net Permeate Activity (cpm)	Net Feed Activity (cpm)	Cummlative Time (hours)	Run	Net Permeate Activity (cpm)	Net Feed Activity (cpm)	Cummlative Time (hours)
14C1	156.1	72004.1	0	14C3	122.1	89520.1	0
	1477.1	87008.1	19		294.1	92618.1	19
	1629.7	42353.7	43		635.7	46185.7	43
	2641.7	43415.7	66		1088.7	47245.7	66
	3296.7	41998.7	91.17		1671.7	48514.7	91.17
	4901.7	42498.7	123.75		2399.7	51550.7	123.75
	5422.7	44226.7	144.5		2866.7	50865.7	144.5
	5817.7	43405.7	162.08		3540.7	51111.7	162.08
	9317.7	45004.7	213		5071.7	54693.7	213
	11661.7	49179.7	260		7566.7	67579.7	260
14C5	121.1	74410.1	0	14C9	114.1	66181.1	0
	1359.1	86150.1	19		273.1	96594.1	19
	1499.7	44558.7	43		994.7	47510.7	43
	2288.7	43445.7	66		1874.7	46812.7	66
	3180.7	41634.7	91.17		3031.7	46397.7	91.17
	4179.7	44666.7	123.75		4436.7	46507.7	123.75
	3678.7	38473.7	144.5		5292.7	46997.7	144.5
	5674.7	46228.7	162.08		6464.7	43705.7	162.08
	7783.7	41771.7	213		8304.7	46175.7	213
	10490.7	48201.7	260		12158.7	54258.7	260